Master Thesis
Flanking Transmission over CLT Joints

Master's Programme in Sound and Vibration

Aleksandra Sadowska
Yanan Liu

DEPARTMENT OF ARCHITECTURE AND CIVIL ENGINEERING

CHALMERS UNIVERSITY OF TECHNOLOGY
Gothenburg, Sweden 2023
www.chalmers.se

Master's thesis 2023

Flanking Transmission over CLT Joints

ALEKSANDRA SADOWSKA
YANAN LIU

CHALMERS
UNIVERSITY OF TECHNOLOGY

Department of Architecture and Civil Engineering
Division of Applied Acoustics
Chalmers University of Technology
Gothenburg, Sweden 2023

Flanking transmission over cross-laminated timber joints
ALEKSANDRA SADOWSKA
YANAN LIU

Supervisor: Andreas Colebring, Efterklang
Examiner: Jens Forssén, Department of Architecture and Civil Engineering

Master's Thesis 2023
Department of Architecture and Civil Engineering
Division of Applied Acoustics
Chalmers University of Technology
SE-412 96 Gothenburg
Telephone +46 31 772 1000

Typeset in LaTeX
Printed by Chalmers Reproservice
Gothenburg, Sweden 2023

Flanking transmission over cross-laminated timber joints

YANAN LIU and ALEKSANDRA SADOWSKA
Department of Architecture and Civil Engineering
Chalmers University of Technology

Abstract

With the rise of cross-laminated timber (CLT) popularity as a construction material, sound transmission control has been considered one of the greatest challenges. Flanking noise transmission over the junction elements takes a high portion of the problem. The existing research is focused on the vibroacoustic aspects of the CLT system, while rather rarely on using the simulation model to predict a specific joint structure.

The thesis was initially aimed to predict the vibration transmission over a certain CLT joint by simulating the model with the finite element method (FEM) and comparing it with the measurement data on-site. Due to the special laminated structure and the orthotropic material properties of cross-laminated timber, correct modeling is challenging. A mode-shapes study of a plain CLT panel was successfully done by testing approaches in both solid and shell modules.

With limited applicable references on FEM modeling of the laminated orthotropic material as well as the shortage of proper boundary condition study, the simulation may not give concrete comparable results, rather it might provide useful hints on the modeling guidelines of CLT elements for the future relevant study.

Keywords: Cross-laminated timber; CLT building; flanking transmission over CLT joints; finite element method modeling;

Acknowledgements

This thesis is a summary work of ours the two years master's study in Sound and Vibration at Chalmers. The whole thesis study was challenging but at the same time a wonderful process. We are very grateful for its completion and all the help we have gotten during this time. We would first give thanks to Andreas Colebring, our supervisor at Efterklang, for his provision of the topic in studying the flanking transmission of CLT structures, and for helping us solve the measurement possibility which is a crucial part of this thesis. We are so appreciative to have Krister Larsson as our extra supervisor who especially guided us in our initial phase of joint modeling. Great thanks to Jens Forssén our examiner for his kind instruction and advice during our work in progress. We want also to thank Anders Hansson the construction-site manager from NCC for enabling us access to the building Magasin X in Uppsala where we could perform the measurement. Warm thanks to our families and friends too, for all the encouragement and support during our time at Chalmers and during the work on the thesis.

Aleksandra Sadowska and Yanan Liu, Gothenburg, January 2023

Contents

List of Figures

List of Tables

1
Introduction

1.1 Background

Cross-laminated timber (CLT) is a popular material in the building industry. It is able to remain high stiffness with low density. Some of the benefits of using CLT are: adaptability to construct different building elements, good seismic resistance, reduced environmental impact and increased economic efficiency. However, the vibroacoustic aspects of this timber system are still under investigation regarding the demand for noise protection, particularly for low frequencies. Among the challenges of the sound transmission control in CLT buildings, flanking noise transmission is addressed even more problematic and complicated. Flanking transmission can give rise to both impact noise from the floor and airborne noise. According to relevant existing research on acoustic issues of CLT structures, the shape (or type) of the joint, as well as the applied fixing technique, take effects critically on the flanking noise insulation in the CLT elements.

1.2 Cross Laminated Timber and the junctions

Cross-laminated timber is a layered wooden structure, made with glued wood slabs. A CLT board usually consists of three, five or seven layers, piled with wooden slabs angled perpendicularly to the direction of the grains in the layer below. Commonly used CLT panels are manufactured with thickness in the range of 80 – 300 mm, width in the range 1.2 – 3 m, and length up to 16 m [16]. In Sweden, spruce or pine is mostly used as a source of wood. The moisture of the wood can vary for different types of glue, but has to lie within the range of 8 – 15 %.

Due the low self-weight CLT panels can be prefabricated and transported easily. Achieving a significant cross-section is possible, which is useful to increase the material stiffness and load-bearing.

Unique properties of CLT are determined by the orthotropic properties of wood [17], meaning that its material properties can differ with x-axis and y-axis. Orthotropic materials are a subcategory of anisotropic materials, in which material properties can differ with direction, contrary to isotropic materials, where material properties remain constant. Since CLT consists of perpendicular layers of wooden slabs, its orthotropic properties might differ when the thickness is changed. The difference in cross section when changing the angle is more significant for a plate build with three

layers than for a seven layers plate. In this thesis it is assumed that orthotropic properties of cross laminated timber dominate isotropic properties, so individual layers are modelled as an orthotropic material.

A CLT panel exhibits great strength properties related to its self weight. Structurally, it behaves similarly to a concrete, but with much lower self weight. Low weight can be an advantage as it makes transportation and assembling easier, but acoustically it is a concern for low frequency acoustic insulation.

A common concern regarding to wooden buildings is fire safety. Wood can ignite, when exposed to fire. Despite this, high fire resistivity can be achieved, due to the fact that a char layer is created on the surface, protecting the inner part [16]. Fire expose behaviour of the wooden structure might be a concern, as its load-bearing properties are reduced. For a CLT panel outer layers and layers parallel with them are considered as load-bearing. Perpendicular layers can transfer shear forces between surrounding layers. Fire handling properties of CLT board are determined by panel thickness, number of boards, as well as type of stress. It was calculated for a floor structure that when between 20 % and 40 % of a load-bearing capacity is used, the structure should remain safe for up to 120 min of standard fire exposure [16].

The aspect that can affect a CLT structure's properties is joint design. It is important not only in terms of load bearing, but also acoustics. The most common ways of connecting CLT boards include using wood screws, metal plates, brackets, anchor nails and screws. Screws are often preferred for tall buildings where joints experience large shear forces.

1.3 Literature review

J Hörnmark, *Acoustics performance of CLT junctions*, 2019 [6]
The calculation and measurement of the vibration reduction index K_{ij} are investigated in the thesis. The measured data are compared with the calculated results based on the method in standard ISO 12354-1 as well as laboratory results from other relevant papers. There are in total four wall-floor junctions measured in-situ including one T-junction and three X-junctions. The thesis got the conclusion that the junction was greatly influenced by the applied load, and the estimation method introduced in ISO 12354-1 did not match well to the in-field measurement results, especially at low frequencies.

F Morandi, *Measurement of flanking transmission for the characterisation and classification of cross laminated timber junctions*, 2018 [14]
This paper gathered results of the measurement work within a project named *flanksound*. Vertical L-, T- and X- junctions and horizontal L-junctions were studied and compared with the calculated data based on the revised edition of the EN ISO 12345:2017. The focus is to investigate the influences of various types and numbers of connections on the vibration reduction indices K_{ij}. In total, 21 connection configurations

were tested.

A continuity test on a vertical X-junction showed that the hierarchy for the energy transmissions were dominated by the relative position and the structural coupling of the joined panels. By testing the same disposition of the panels but with different connection methods, the paper obtains that with increased number of CLT elements in the junction less obvious differences appear in the flanking transmission; and for a certain flanking path, the fastening method influenced greatly on the consistency of the tendency of transmission change in the frequency range.

A Di Bella, *Acoustic characteristics of cross-laminated timber systems*, 2020 [4]
This is a paper review, presenting a large amount of relevant research results on the acoustic characteristics of CLT timber structures, including the basic components' interactions through the joints addressed. The author mentioned that obtaining the radiation efficiency of CLT panels is important for predicting the panels' vibration behaviour and lateral transmission effects.

1.4 Aim

The theme of the thesis covers quite challenging study aspects about the specific building material of CLT related to its acoustic characteristics. The study process as well as outcome has later redefined and narrowed the goal of our thesis. We have basically built up a simple CLT joint model with its special orthotropic and layered structure; with setting very basic and general boundary conditions we studied the theoretical model behavior and compared it with the measurement results.

The goal of the thesis including:

1. investigation of the flanking sound transmission over a few typical joints of CLT panels;
2. studies of reliable prediction models for simulating the joints' acoustic performances, with a focus on the determination of the vibration reduction index, Kij.

1.5 Methods

Flanking transmission is a complicated issue, where several factors need to be considered, which makes theoretical calculations less reliable due to inevitable simplifications. Finite Element Modelling (FEM) as a simulation method will be applied to approximate the behavior of the test structure, mainly for obtaining results at low frequencies range.

Flanking sound transmission and vibration propagation transfer function for the certain types of joints will also be measured in a CLT building. The measurement

results will be used to compare with the data obtained by simulation. Since the sound transmission is the most troublesome for low frequencies, the range of 20 –200 Hz will be prioritized in the modeling.

2
Theory

2.1 Sound and vibration

Sound is a sensation perceived by the brain as a result of acoustical waves detected by the ears. It can be also defined as vibration propagated by acoustical waves itself [13]. Sound waves are longitudinal motions in gas or liquids, in the direction of sound propagation, which means for the particles in the media, the only movement that occurs is compression and decompression.

To create a sound wave, a source of vibrations is needed. When an object is excited by a force, it vibrates. After the elimination of the force, stored energy causes oscillation for certain frequencies, called resonance frequencies [13]. To reduce the oscillation amplitude, damping is necessary. Other ways of removing energy from the vibrating structure are friction and radiation. Due to radiation, energy is transformed into sound waves. The purpose of this thesis is to investigate structural vibration, which leads to sound radiation.

2.2 Waves in solids

In solid media, sound and vibrations are propagated in different wave types than just longitudinal waves. Mostly the wave motion in solids is a result of a combination of longitudinal and transverse waves.

2.2.1 Quasi-longitudinal waves

In reality, no pure longitudinal waves exist in a finite structure. In an actual building structure, a longitudinal wave propagation will result in lateral displacement on the surface, such wave type is named quasi-longitudinal waves, see Figure 2.1 a). The related wave speed, propagating in one direction can be calculated as [10]

$$c_L = \sqrt{\frac{D}{\rho}} \, . \tag{2.1}$$

For the waves in rods, it has:

$$D = E \tag{2.2}$$

where E is Young's modulus of the material in Pascals and ρ is the density of the material in kg/m^3.

For a plate where the wave propagation occurs in two directions x and y, the corresponding strains are related to each other according to [10]:

$$|\epsilon_x| = \mu|\epsilon_y| \tag{2.3}$$

where μ is Poisson's number. And thus

$$D = \frac{E}{1-\mu^2} \, . \tag{2.4}$$

The speed of the longitudinal waves in a plate is then expressed as

$$c_{L,xy} = \sqrt{\frac{E}{\rho(1-\mu^2)}} \, . \tag{2.5}$$

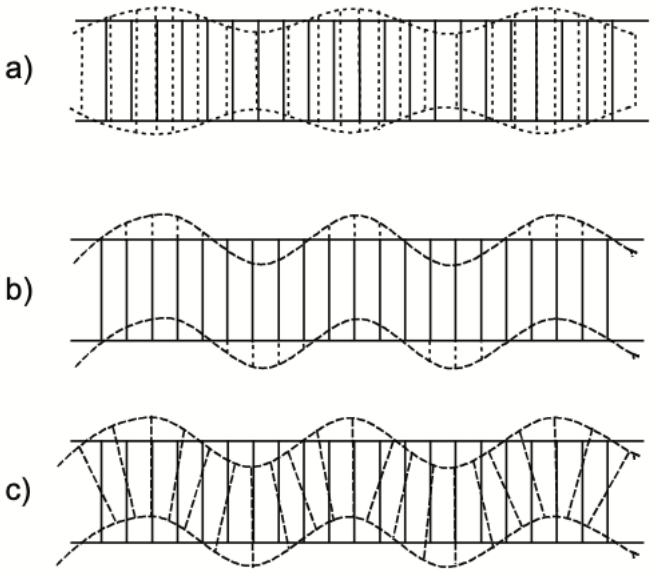

Figure 2.1: Wave types in solids. a) Quasi-longitudinal wave. b) Transverse wave. c) Bending wave [17].

2.2.2 Transversal waves

For wave propagation in solids, another type of wave can be distinguished. Transversal waves cause a change in shape with constant volume, contrary to longitudinal waves, which affect the volume. For transversal wave shear modulus, G is used to describe the elastic properties of the material. The speed of sound can be calculated accordingly, for the dimensional case:

$$c_T = \sqrt{\frac{G}{\rho}} \, . \tag{2.6}$$

Shear modulus G can be calculated as a function of Young's modulus, with the use of Poisson's number:

$$G = \frac{E}{2(1+\mu)} \tag{2.7}$$

2.2.3 Bending waves

The most crucial for sound radiation are bending waves. This type of wave is more likely to be excited, as they cause the structure's displacement in the direction normal to the surface. When describing bending waves, some simplifications are usually applied.

For the bending waves propagating in a beam, a bending angle can be defined according to the Euler-Bernoulli theory as

$$\beta = \frac{\partial \eta}{\partial x} \tag{2.8}$$

where η is displacement in normal direction and x is the length of the element. The bending moment caused by the bending angle can be expressed as [10]

$$M = -B\frac{\partial \beta}{\partial x} = -B\frac{\partial^2 \eta}{\partial x^2} \tag{2.9}$$

where B is the bending stiffness. If two bending moments are applied to the body, the force at the cross-section can be written as

$$F = -\frac{\partial M}{\partial x} = \frac{\partial}{\partial x} B\frac{\partial^2 \eta}{\partial x^2} \, . \tag{2.10}$$

If a particle in the body is considered, it is accelerated by the net force applied to it - the force is changing over the dimension. According to Newton's law, this force can be expressed as

$$\frac{\partial F}{\partial x} = m\frac{\partial^2 \eta}{\partial t^2} \tag{2.11}$$

where m is mass per unit length.

Combining Equation 2.10 and Equation 2.11, the wave equation is obtained as

$$\frac{\partial^2}{\partial x^2}\left(B(x)\frac{\partial^2 \eta}{\partial x^2}\right) + m\frac{\partial^2 \eta}{\partial t^2} = 0 \, . \tag{2.12}$$

Assuming constant bending stiffness, the above equation can be simplified to

$$B\frac{\partial^4 \eta}{\partial x^4} + m\frac{\partial^2 \eta}{\partial t^2} = 0 \, . \tag{2.13}$$

The solution of the wave equation has to be in the wave form, $\eta(\mathrm{x,t}) = \eta_A e^{-jkx} e^{j\omega t}$. Equation 2.13 can be written as

$$(Bk^4 - \omega^2 m)\eta_A = 0 \, . \tag{2.14}$$

The non-trivial solution of the above equation is

$$k^4 = \frac{\omega^2 m}{B} \tag{2.15}$$

what leads to four solutions, representing waves in two directions and two near-fields. The speed of the bending waves can be then calculated as

$$c_B = \sqrt[4]{\frac{B}{m}\omega^2} \tag{2.16}$$

For an isotropic material plate with density ρ in kg/m^3 and having thickness h, with subsituting the bending stiffness B as

$$B = \frac{E}{1-\mu^2} I \tag{2.17}$$

where I is the area moment of inertia, given as $I = h^3/12$
and with $m = \rho \cdot h$. The bending wave speed can also be calculated as

$$c_B = \sqrt{\frac{\pi}{\sqrt{3}} c_L h f} \tag{2.18}$$

where the speed of longitudinal wave c_L is given in Equation 2.5.

2.3 Modal analysis

Each structure reacts to excitation in an individual way, determined by the material, the shape, and boundary conditions. Excitation of certain frequencies (eigenfrequencies) is more significant than others. Each of them has an established vibration pattern - eigenfunction. The behavior of the structure can be studied through the study of individual modes.

2.3.1 Eigenfrequencies of isotropic plates

An equation describing the modes of an isotropic plate can be obtained by satisfying the boundary conditions and the wave equation. In the equation, the displacement of points on the plate is calculated. For a simply supported plate in the x-y plane, the bending mode shape is expressed as [3]

$$\psi_{p,q} = sin\left(\frac{p\pi x}{L_x}\right) sin\left(\frac{q\pi y}{L_y}\right) \tag{2.19}$$

where p, q are mode numbers, L_x and L_y are lengths of the plate in respective directions in meters and x and y are positions in respective directions, in meters.
To calculate frequencies for which modes occur, it is useful to visualize a plate as two beams, on axis x and y respectively. For a beam, modes occur when the wave number is in the form of [3]

$$k_B^2 = \left(\frac{p\pi}{L_x}\right)^2 \tag{2.20}$$

where p is a positive integer and L_x is the length of the beam in m. The same principle is applicable to the y-axis. The wave number for modes in plates is then

$$k_B^2 = \left(\frac{p\pi}{L_x}\right)^2 + \left(\frac{q\pi}{L_y}\right)^2 . \tag{2.21}$$

Combining the equation above and Equation 2.15, the related eigenfrequencies can be calculated as

$$f_{p,q} = \frac{c_B}{2}\sqrt{\left(\frac{p}{L_x}\right)^2 + \left(\frac{q}{L_y}\right)^2}\,. \tag{2.22}$$

2.3.2 Eigenfrequencies of orthotropic plates

Cross-laminated timber is a type of orthotropic material, which means that its material properties vary along the three orthogonal axes. This means the material properties e.g. Young's modulus and Poisson's ratio differ along the corresponding axes, and hence different bending stiffness and wave propagation speed. The wave equation can be written as

$$B_x\frac{\partial^4\eta}{\partial x^4} + 2B_{xy}\frac{\partial^4\eta}{\partial x^2\partial y^2} + B_y\frac{\partial^4\eta}{\partial y^4} + m\frac{\partial^2\eta}{\partial t^2} = 0 \tag{2.23}$$

where B_x, B_y represent the bending stiffness in the x- and y-directions, B_{xy} is a mixed term [5].

The vibrational pattern of orthogonal structures can be expressed as the superposition of individual modes [10]. For a rectangular and simply supported orthotropic plate with thickness h, the corresponding Young's modulus E_x, E_y and Possion's ratio μ_x, μ_y will satisfy [17]

$$E_x\mu_y = E_y\mu_x \tag{2.24}$$

Accordingly, the bending stiffness B_x and B_y will then become as

$$B_x = \frac{E_x h^3}{12\left(1-\mu_x\mu_y\right)} \tag{2.25}$$

and

$$B_y = \frac{E_y h^3}{12\left(1-\mu_x\mu_y\right)} \tag{2.26}$$

Similar to the equation 2.22 for the homogeneous plates, the eigenfrequencies for orthotropic plates can be written as [5]

$$f_{p,q(O)} = \frac{\pi}{2\sqrt{m}}\left[\sqrt{B_x}\left(\frac{p}{L_x}\right)^2 + \sqrt{B_y}\left(\frac{q}{L_y}\right)^2\right]\,. \tag{2.27}$$

With substituting B_x and B_y using equation 2.25 and 2.26, and expressing the Youngs moduli E_x, E_y with longitudinal wave speed $c_{L,x}$, $c_{L,y}$ using equation 2.5, equation 2.27 can also be written as

$$f_{p,q(O)} = \frac{\pi h}{2\sqrt{12}}\left[c_{L,x}\left(\frac{p}{L_x}\right)^2 + c_{L,y}\left(\frac{q}{L_y}\right)^2\right] \tag{2.28}$$

Sometimes the elastic properties of orthotropic materials can be approximated to gain a general idea of the eigenfrequencies. For example, since CLT plates contain an

odd number of layers, the bending stiffness for the main direction can be assumed to be dominating, especially for plates that contain a small number of layers. Another approach is to calculate an effective bending stiffness B_{eff}, which is a geometric mean of the bending stiffness in two directions [3]

$$B_{xy} \approx B_{eff} = \sqrt{B_x B_y} \tag{2.29}$$

2.3.3 Modal density and modal overlap factor

Modal density describes the number of eigenfrequencies that occur for a certain frequency band. Evaluation of modal density is of importance when energy storage of modes might affect the results. In a simple method of evaluating modal density, a plate is assumed to be simply supported or clamped, so that there are no modes on axes [3].

The wave number for a plate can be expressed by wave number components in respective axes, k_{ix}^2 and k_{ny}^2

$$k_{i,n}^2 = k_{ix}^2 + k_{ny}^2 \tag{2.30}$$

Each eigenfrequency can be shown as a point on a lattice, as shown in the figure below.

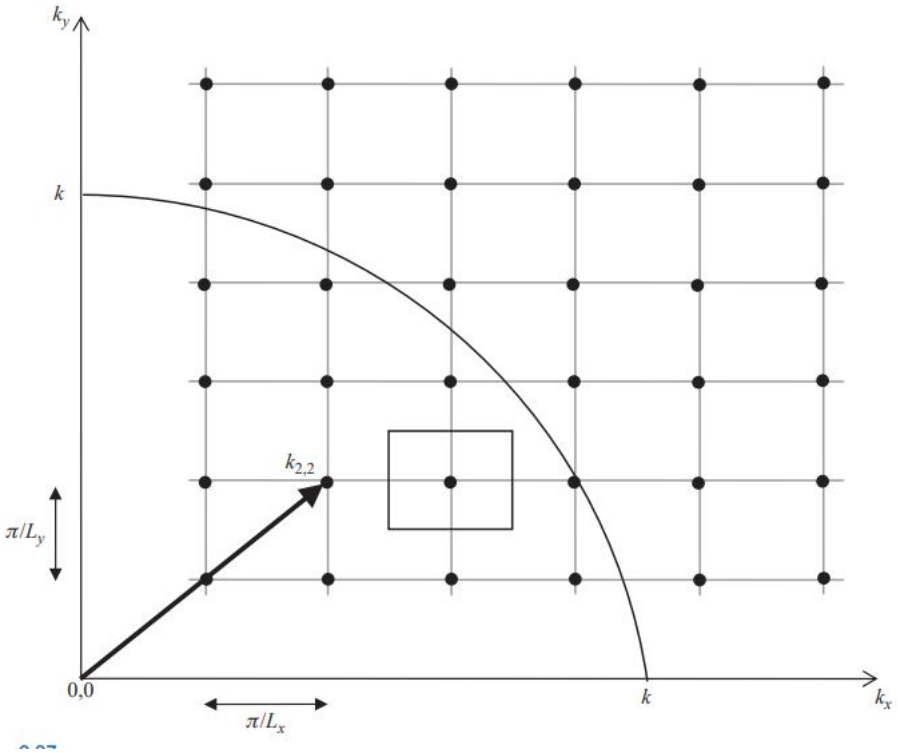

Figure 2.2: Modes for a two-dimensional simply supported plate. An exemplary vector corresponding to an eigenvalue is shown [3]

The number of modes per frequency interval can be calculated as the number of modes between two vectors, corresponding to frequencies defining the given interval.

The total number of modes is:

$$N = \frac{k_B^2 S}{4\pi} = \frac{\omega S}{3.6 c_L h} \tag{2.31}$$

where S is the plate surface area in m^2, c_L is the speed of sound for longitudinal waves, h is the thickness of the plate in m [11]. The number of modes per frequency range, or modal density, is then:

$$\frac{\Delta N}{\Delta \omega} = \frac{S}{3.6 c_L h} \tag{2.32}$$

Modes of the structure were presented as independent points. However, for real-life structures with damping present, modes have a certain width and can be exceeded for frequencies close to the eigenfrequency, but not exactly equal to it. As a result, certain forces might exceed two or more nodes. The modal overlap factor describes if and how much of the modes overlap. It is calculated as

$$M = \frac{\Delta f_{3\ \mathrm{dB}}}{\Delta f} = f \cdot \eta_{tot} \cdot n \tag{2.33}$$

where $\Delta f_{3\ \mathrm{dB}}$ is the spacing between two points with a level lower than the peak level by 3 dB, which is also called half-power bandwidth, Δf is the average spacing between modes, η_{tot} is total loss factor and n is the modal density.

2.4 Damping

Damping occurs when vibrational energy is transformed into other forms of energy. It can be divided into material and non-material damping. Examples of non-material damping are sound radiation, and viscous friction between surfaces [10].

The losses in the structure can be evaluated by the use of the loss factor η, which describes the ratio of the energy that is lost. When considering vibration propagation in the structure, the total loss factor η_{tot} can be evaluated based on structural reverberation time [9]:

$$T_s = \frac{2.2}{f \cdot \eta_{tot}} \tag{2.34}$$

where f is the band central frequency in Hz and T_s is structural reverberation time. A detailed description of structural reverberation time measurement is presented in Section 3.1.3.

The total loss factor consists of the internal loss factor, describing material damping, and the coupling loss factor, describing non-material damping. For a plate, it can be expressed as [9]:

$$\eta_{tot} = \eta_{int} + \frac{2\rho_0 c_0 \sigma}{2\pi f m'} + \frac{c_0}{\pi^2 S \sqrt{f \cdot f_c}} \sum_{k=1}^{4} l_k \alpha_k \tag{2.35}$$

where η_{int} is the internal loss factor of the material, m' is the mass per unit area, in kg/m^2, σ is the radiation factor for bending waves, f_c is the critical frequency, in Hz, and calculated as

$$f_c = \frac{c_0^2}{1.8 c_L t} \tag{2.36}$$

and l_k is the length of the junction at the perimeter k, α_k is the absorption coefficient for bending waves at the perimeter k.

The three components in the equation 2.35 represent the internal loss factor, radiation losses, and absorption, respectively. The internal loss factor for a given material can be found in the literature, but for homogeneous building materials, a common approximation of 0.01 is applied. The loss factor due to radiation is commonly neglected [9]. The absorption coefficient is characteristic of a certain situation.

2.5 Driving point mobility

When an impact sound e.g. footstep noise is perceived by people meaning a certain form of vibration is generated in the building structure, namely structure-borne sound. The force applied to the structure has caused velocities (and velocity distribution) over the structure. Structures with different forms, sizes, or material compositions will respond differently to a given force excitation.

2.5.1 Simple mass-spring system

An important dynamic quantity to study a system's response to an external force is mobility, calculated as the ratio (in complex value) of the induced velocity and the point force at single frequencies. When the velocity is obtained at the same point as the excitation, the quantity is named driving point mobility or input mobility; with velocity obtained at any other point is called transfer mobility. Both items describe the reaction at a certain point with respect to the force excitation. Normally transfer mobility is used to define the vibration resonances of a structure, while the driving point mobility also gives information on the power input to the system of the given force.

Taking a harmonic force $F(t)$ applied on a simple mass-spring system as an example is show in the figure below. $F(t)$ is expressed as

$$F(t) = \hat{F} e^{j(\omega t + \phi)} \tag{2.37}$$

where $\hat{F}$ is the force amplitude, ω is the angular frequency, ϕ is the initial phase.

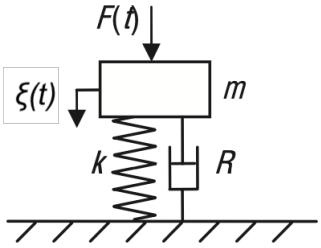

Figure 2.3: A mass-spring system [5]

The differential equation of this system's motion is

$$F(t) = m\frac{d^2\xi}{dt^2} + R\frac{d\xi}{dt} + k\xi \tag{2.38}$$

of where ξ is the vertical displacement, m is the mass, R is the damping coefficient, k is the spring stiffness.

Since harmonic force will also give rise to harmonic velocity $v(t)$, with expressing $\xi(t)$ by $v(t)$, the above equation can be rewritten as

$$F(t) = \left[R + j\left(\omega m - \frac{k}{\omega}\right)\right] v(t) \ . \tag{2.39}$$

According to the definition, the driving point mobility is then given as

$$Y = \frac{v}{F} = \frac{1}{R + j\left(\omega m - \frac{k}{\omega}\right)} \ . \tag{2.40}$$

For an undamped case - meaning R equals to 0, the eigenfrequency ω_0 of the system will satisfy

$$\omega_0^2 m - k = 0 \ . \tag{2.41}$$

With the relation between the damping coefficient R and the loss factor η having $R = \eta\sqrt{km}$, the R term in the driving point mobility 2.40 can be replaced and get

$$Y = \frac{v}{F} = \frac{1}{\eta\omega_0 m + j\left(\omega m - \frac{k}{\omega}\right)} \ . \tag{2.42}$$

The corresponding power input is calculated as [3]

$$W_{in} = \frac{1}{2}Re\{Fv^*\} = \frac{1}{2}\hat{F}^2 Re\{Y\} = \tilde{F}^2 Re\{Y\} = \tilde{F}^2\eta\omega_0 m\hat{Y}^2 \tag{2.43}$$

where $*$ is the notion for the complex conjugate. The $\hat{F}$ and $\hat{Y}$ represent the magnitude of the excitation force and driving-point mobility. In the (or nearly) undamped case i.e. $\eta < 0.3$, the peaks of both the real part or the magnitude of Y appear at the resonance frequency $f_0 = \frac{\omega_0}{2\pi} = \frac{1}{2\pi}\sqrt{\frac{k}{m}}$.

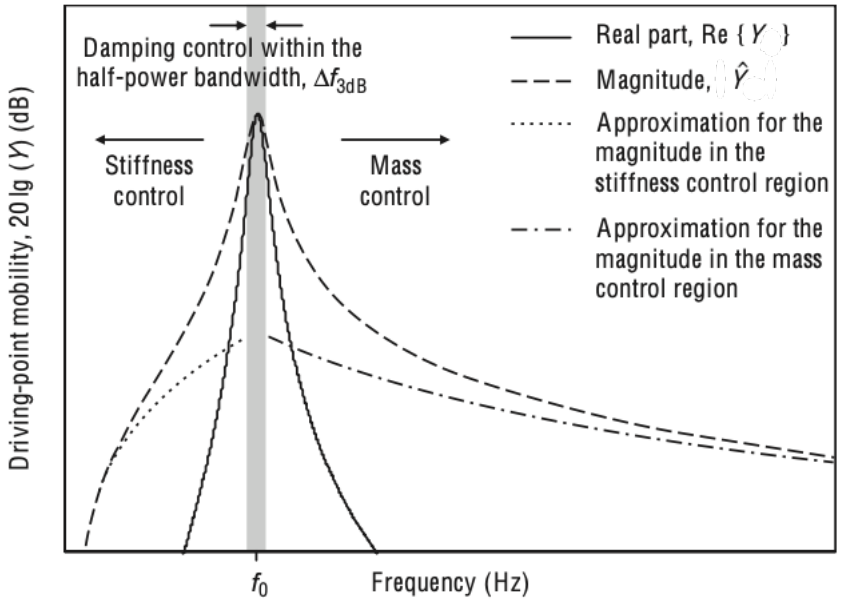

Figure 2.4: Driving-point mobility of a mass-spring system [5]

Figure 2.4 shows a driving-point mobility in decibels of a simple mass-spring system. The half-power bandwidth – 3 dB down from the peak level is the damping controlled area for the input mobility magnitude $\hat{Y}$. Below the frequency, f_0 the driving-point mobility is under stiffness control, and it can be estimated according to equation 2.40 as

$$Y \approx j\frac{\omega}{k} \,. \tag{2.44}$$

Similarly, the mass-controlled region of Y at high frequencies gives

$$Y \approx \frac{1}{j\omega m} \,. \tag{2.45}$$

2.5.2 Input mobility of finite plates

For a simply supported rectangular plate, with considering only bending waves by a point force applied normally to the surface, the vibrational response can be estimated as the composition of all the single modes. Accordingly, the driving-point mobility at the point (x,y) on the plate can be calculated as [3]

$$Y = \frac{j4\omega}{m} \sum_{p=1}^{\infty} \sum_{q=1}^{\infty} \frac{\psi_{p,q}^2(x,y)}{\omega_{p,q}^2(1+j\eta) - \omega^2} \tag{2.46}$$

where the bending mode shape $\psi_{p,q}$ is given by Equation 2.19 and $\omega_{p,q}$ is the corresponding angular mode frequency.

2.5.3 Input mobility of infinite plates

For excitation on infinite plates (considering also bending wave vibration), the input mobility is given by

$$M_\infty = \frac{1}{8\sqrt{m \cdot B}} \,. \tag{2.47}$$

It is obvious to see that M_∞ becomes a real number and frequency independent. In fact, this quantity also approximates the average mobility of a finite plate (of the same material) over different input positions and frequencies.

2.5.4 Vibration fields in building structures

In building acoustics frequencies, the vibration field is mostly referred to as a diffuse field, especially above the lowest eigenfrequency. In practical measurements, spatially averaged vibration level (by frequency) is determined by taking several random positions on the structure.
Vibration analysis of most building structures is far more complex due to the interaction between connected structures. The vibration behavior will be dominated both by the modes of singular elements and the global modes of the coupled system. To model the vibration of coupled elements, Statistical Energy Analysis (SEA) can be used to estimate the local modes, and Finite Element Method (FEM) can be used to study the global modes.

2.6 Sound radiation

Sound radiation is a mechanism of transforming the vibrational energy of a structure into a sound wave. The efficiency of this mechanism is defined by the radiation factor [11]:

$$\sigma = \frac{W}{\rho c S \langle \tilde{v}^2 \rangle} \tag{2.48}$$

where W is radiated power in W, S is surface area in m^2, $\langle \tilde{v}^2 \rangle$ is the spatially averaged mean square velocity of the structure and ρc is the characteristic impedance of the surrounding medium i.e. air. Radiation factor can be also called radiation efficiency or radiation ratio [17]. And sound radiation related to the bending wave field will be focused as our theory base.

2.6.1 Radiation of infinite plates

To understand radiation mechanisms, an infinite plate can be considered first. The velocity of the plate is given as:

$$v_B = \hat{v} e^{j(\omega t - k_B x)} \tag{2.49}$$

where $\hat{v}$ is the amplitude and k_B is the wave number for the bending wave propagating in x direction. Sound pressure in the surrounding medium can be expressed

as

$$p(x,y) = \hat{p}e^{j(\omega t - k_x x - k_y y)} \tag{2.50}$$

where k_x and k_y are wave number components for the surrounding medium. Since the equation 2.50 has to be a solution of the classical wave equation, the wave number of the sound field above the plate is

$$k = \frac{\omega}{c_0} = \sqrt{k_x^2 + k_y^2} \tag{2.51}$$

The condition for sound propagation is that the component of particle velocity normal to the surface v_y has to be equal to v_B. The v_y component is [17]

$$v_y = -\frac{1}{j\omega\rho_0} \cdot \frac{\partial p}{\partial y} = \frac{\hat{p}k_y}{\rho_0\omega} e^{j(\omega t - k_x x - k_y y)} \tag{2.52}$$

and for $y = 0$, on the surface of the plate

$$\hat{v} \cdot e^{-jk_B x} = \frac{\hat{p}k_y}{\rho_0\omega} e^{-jk_x x} \tag{2.53}$$

for this equation to be met,

$$\hat{p} = \frac{\rho_0\omega}{k_y} \cdot \hat{v} \text{ and } k_x = k_B \tag{2.54}$$

The sound pressure can be then written as

$$p(x,y) = \frac{\rho_0 c_0 \hat{v}}{\sqrt{1 - \frac{k_B^2}{k^2}}} e^{j(\omega t - k_B x)} e^{j\sqrt{k^2 - k_B^2}y} \tag{2.55}$$

With the sound pressure expressed in Equation 2.55, two intervals of k_B can be distinguished - $k_B < k$ and $k_B > k$. When the bending wave number k_B is greater than the wave number of the surrounding medium k, the exponent containing y becomes a real number and the sound pressure will be only due to exponentially decreasing with the distance near field.

For the opposite case, the sound wave will be an ordinary propagating plane wave, with sound pressure increasing with a ratio of k/k_B. This ratio determines the angle of propagation φ:

$$\frac{k}{k_B} = \frac{1}{sin\varphi} \tag{2.56}$$

2.6.2 Critical frequency of a plate

A sound wave can be radiated from a structure for a certain ratio of wave numbers in the structure and the surrounding medium, as described above. Connected with the ratio of wave numbers is the ratio of wavelengths. The wave in the structure has to be able to fit into the surrounding medium, at a certain angle. This condition is called *trace matching* and is shown in the figure below [17]. The driving point mobility is

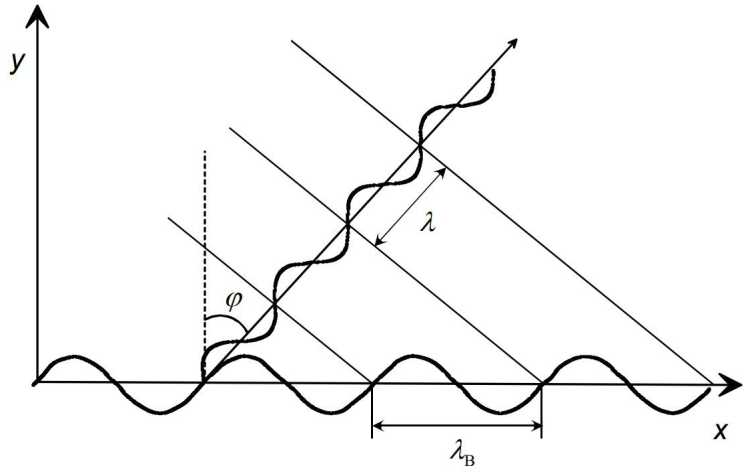

Figure 2.5: Relationship between the wavelength in the structure and the surrounding medium [17].

The maximum wavelength that would be able to fit into the surrounding is the same length as in the structure. It means that the phase speed in the plate c_B is the same as the phase speed in the surrounding medium c_0:

$$c_0 = \sqrt{\omega} \cdot \sqrt[4]{\frac{B}{m}} \tag{2.57}$$

Solving the Equation 2.57 with respect to frequency, the lowest frequency for which sound wave radiation can occur is

$$f_c = \frac{c_0^2}{2\pi}\sqrt{\frac{m}{B}} \tag{2.58}$$

This frequency is called critical frequency. It is worth noting that for orthotropic plates two critical frequencies occur, for propagation in the x and y-axis. To calculate effective critical frequency, effective bending stiffness B is used in Equation 2.58.

2.6.3 Radiation of finite plate

Radiation of a finite plate is more complicated than for an idealized, infinite case. The behavior of the plate is dominated by its modes. Radiated power can not be calculated based on the material properties and dimensions only, the excitation is needed too. However, the behavior related to an individual mode is more straightforward. It can be studied through Rayleigh's integral. A vibrating plate can be approximated as a continuous field of sound sources. The sound pressure or a one-dimensional case is then expressed as

$$p(R,\omega) = \frac{j\omega\rho_0}{2\pi}\frac{e^{-jk_0R}}{R}v(k_x) \tag{2.59}$$

where R is the distance between the center of the plate and the receiving point, in m. For the two-dimensional case, the vibration pattern on the plate is given as [10]

$$v_p(x,y) = v_0 sin(\frac{p\pi}{a}x) sin(\frac{q\pi}{b}y) \tag{2.60}$$

where p and q are plate dimensions. Corresponding wavenumbers are

$$k_{x,y} = \sqrt{k_x^2 + k_y^2}. \tag{2.61}$$

The wavenumbers above can be used to divide modes on plates into three groups:

- Surface modes, where $k_x, k_y < k$
- Edge modes, where $k_x > k > k_y$ or $k_y > k > k_x$
- Corner modes, where $k_x, k_y > k$

Calculation of the radiation efficiency for a finite plate is cumbersome, but certain approximations are given in the literature [10]:

$$\sigma = \begin{cases} \sigma_1 = \frac{\lambda_c^2}{S}(2g_1 + \frac{U}{\lambda_c}g_2) & \text{for } f < f_c \\ \sigma_2 = \sqrt{L_x/\lambda_c} + \sqrt{L_y/\lambda_c} & \text{for } f \approx f_c \\ \sigma_3 = 1/\sqrt{1-(f_c/f)} \text{ if } \sigma_3 < \sigma_2 & \text{for } f > f_c \end{cases} \tag{2.62}$$

where $U = 2(L_x + L_y)$, $S = L_x L_y$, and parameters g_1 and g_2 are expressed as

$$g_1 = \begin{cases} \frac{4}{\pi^4}(1 - \frac{2f}{f_c}))\frac{1}{\sqrt{1-f/f_c}} & \text{for } f < 0.5 f_c \\ 0 & \text{for } f > 0.5 f_c \end{cases}$$

$$g_2 = \frac{1}{4\pi^4} \frac{(1 - f/f_c)\ln(\frac{1+f/f_c}{1-f/f_c}) + 2\sqrt{f/f_c}}{(1-f/f_c)^{3/2}}$$

These approximations are only valid with certain assumptions, such as simply supported plate in an infinite baffle, point excitation, the amplitudes of modes are similar and the size of the plate is at least a quarter of the wavelength in air.

2.7 Vibration transmission over junctions

A significant contribution to overall noise transmission in buildings is due to vibration transmission through partitions. It is more complicated to predict than direct transmissions, mostly because of certain variations in construction, caused by the imperfectness of workmanship and material properties [3]. There are also many possible paths of transmission, which makes the prediction of real-life behavior more complicated. It is important to keep these limitations in mind when analyzing vibration transmission in buildings, as significant uncertainties might occur.

The most significant type of wave for vibration transmission is bending waves. For adjacent rooms, studying bending waves only is sufficient to predict vibration transmission [3]. Plate junctions can be idealized as one of the types: a rigid junction with plates either rigidly connected together or rigidly connected to a beam or column, connection via a resilient material, or a hinged junction. The most popular

model is a rigid junction.

Junctions are often described by their shape, and the way in which plates are connected. The most popular joint constructions are shown in the figure below.

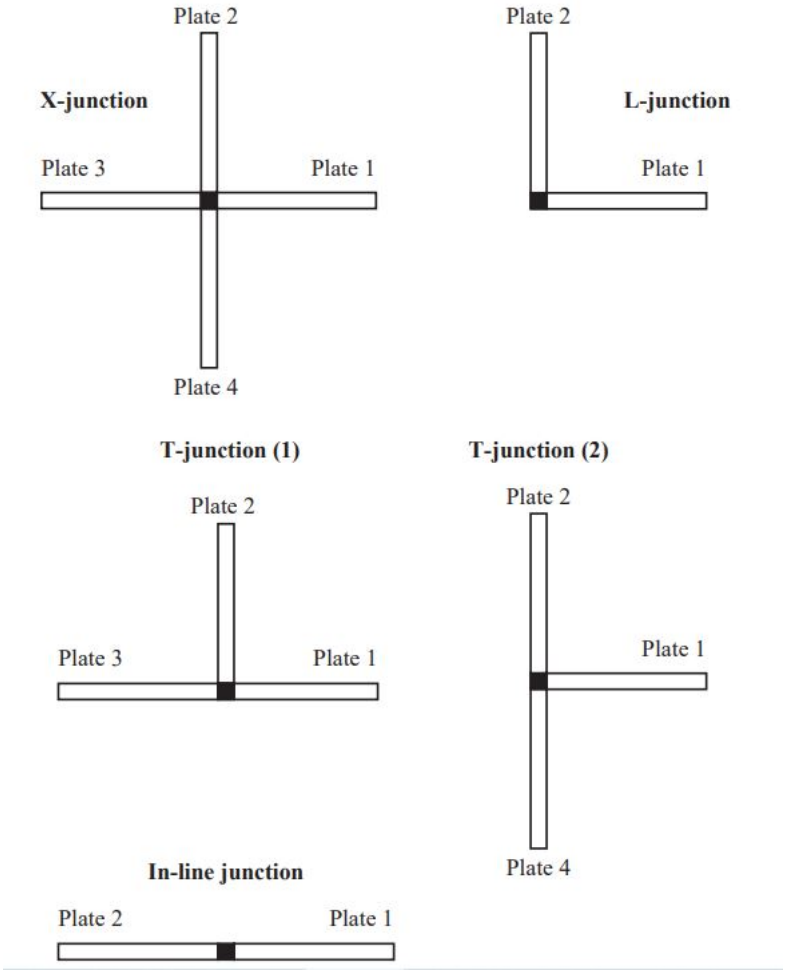

Figure 2.6: Exemplary constructions of joints [3].

2.7.1 Flanking transmission

Any non-direct sound transmission is called *flanking transmission*. Vibration transmission is the main mechanism of flanking transmission. To evaluate the level of flanking, an analysis of vibration transmission is needed.

Vibration transmission can be evaluated by using the transmission coefficient

$$\tau_{ij} = \frac{W_{ij}}{W_{\mathrm{inc},i}} \tag{2.63}$$

where W_{ij} is the power transmitted across the junction and $W_{\mathrm{inc},i}$ is the incident power, which gives transmission loss in decibels as [3]

$$TL = 10\log(\frac{1}{\tau_{ij}}) \ . \tag{2.64}$$

The wave approach assumes a certain angle of incidence θ. Transmission coefficient is angle specific then – $\tau_{ij}(\sigma)$. However, with the diffuse vibration field i.e. above the first eigenfrequency 2.5.4, all angles of incidence can occur with the same probability. To get a rough estimation of the angular averaged transmission coefficient, the normal transmission coefficient can be used.

Transmission over joint has to fulfill Snell's law of refraction. The angle of incidence and the angle of transmission are related as

$$k_j sin(\theta_i) = k_i sin(\theta_j) \tag{2.65}$$

where θ_i is the angle of incidence and θ_j is the angle of transmission.
The transmission coefficient can be calculated for some basic joint constructions. It is assumed that plates that are in-line are made with identical materials and perpendicular plates differ [3]. To simplify further calculations, two variables are introduced:

$$\chi = \frac{k_{B2}}{k_{B1}} = \frac{\sqrt[4]{\rho_{S2}B_1}}{\sqrt[4]{\rho_{S1}B_2}} = \sqrt{\frac{f_{c2}}{f_{c1}}} \tag{2.66}$$

$$\psi = \frac{B_2 k_{B2}^2}{B_1 k_{B1}^2} = \frac{h_2 c_{L2} \rho_{s2}}{h_1 c_{L1} \rho_{s1}} = \frac{\rho_{s2} f_{c1}}{\rho_{s1} f_{c2}} \tag{2.67}$$

where indices 1 and 2 refer to the properties of respective plates. The transmission coefficient over the corner, so between perpendicular plates for an X joint or a T joint can be calculated according to the equation [11]

$$\tau_{ij}(\sigma) = \frac{0.5 J_1 J_2 \psi \cos\sigma \sqrt{\chi^2 - \sin^2\sigma}}{(J_2\psi)^2 + \chi^2 + J_2\chi(\sqrt{1+\sin^2\sigma}\sqrt{\chi^2+\sin^2\sigma} + \sqrt{1-\sin^2\sigma}\sqrt{\chi^2-\sin^2\sigma})} \tag{2.68}$$

for $\chi \geq \sin\sigma$, $\tau_{ij}(\sigma) = 0$ otherwise. Parameters J_1 and J_2 depend on the junction construction, for a X joint $J_1 = J_2 = 1$, for T junctions $J_1 = 2$ and $J_2 = 0.5$ for construction 1 in Figure 2.6, and $J_1 = J_2 = 2$ for T joint construction 2 in Figure 2.6.

Despite simplifications and assumptions applied, calculations remain complicated and give significant uncertainties. For more complex structures, Statistical Energy Analysis and Finite Element Method are widely used. To study the transmission at low frequencies, which is the focus of this thesis, Finite Element Method is a better choice. It will be described in detail in the next chapter.

3

Field measurement

3.1 Measurement theory and methods

The measurement was done according to the standard ISO 10848-1 [8] which covers the description for the in-field measurement for flanking transmission of building components.

3.1.1 Vibration reduction index K_{ij}

As a type of solid wood product, CLT has been defined as a Type A element (referring to ISO 10848-1). The main index for the characterization of vibration transmission over a joint made of CLT is the vibration reduction index K_{ij}. K_{ij} is defined in the standard ISO 12354-1 [9] as an invariant quantity to evaluate the vibrational power transmission between structural elements across a junction. It is measured by using structural-borne excitation and calculated by normalizing the direction-averaged vibration level difference over the junction, given as

$$K_{ij} = \overline{D_{v,ij}} + 10\log\left(\frac{l_{ij}}{\sqrt{a_i a_j}}\right) \tag{3.1}$$

where $\overline{D_{v,ij}}$ is the direction-averaged vibration level difference, expressed in decibels; l_{ij} is the common length in the junction between the two elements, in meters; a_i,a_j are the equivalent absorption lengths, expressed in meters, which are related to the structural reverberation time T_s of elements i and j as follows,

$$a_i = \frac{2.2\pi^2 S_i}{T_{s,i} c_0 \sqrt{\frac{f}{f_{ref}}}} \tag{3.2}$$

where $T_{s,i}$ is the structure reverberation time of element i, in seconds; S_i is the surface area of element i, in m^2; c_0 is the sound speed in air, in m/s; f is the frequency, in Hz; f_{ref} is the reference frequency, set as 1000 Hz.

The measurement for $\overline{D_{v,ij}}$ and a_i,a_j (namely by determining $T_{s,i}$, $T_{s,j}$) will be introduced in the following subsections.

3.1.2 Direction-averaged velocity level difference $\overline{D_{v,ij}}$

$\overline{D_{v,ij}}$ is the average of the velocity level difference between two elements in both directions across a junction, given as

$$\overline{D_{v,ij}} = \frac{1}{2}\left(D_{v,ij} + D_{v,ji}\right) \tag{3.3}$$

where $D_{v,ij}(/D_{v,ji})$ is defined as the level difference of the time and space averaged mean-square normal velocity between element $i(/j)$ and element $j(/i)$, when only the element $i(/j)$ is excited.

In the circumstance of airborne or steady-state structure-borne excitation, the average velocity level L_v is calculated as

$$L_v = 10log\left(\frac{\frac{1}{T_{int}}\int_0^{T_{int}}\left({v_1}^2(t) + {v_2}^2(t) + ... + {v_n}^2(t)\right)dt}{n \cdot {v_0}^2}\right) \tag{3.4}$$

where v_1, v_2, v_n are r.m.s. velocities, expressed in m/s, at n different measurement positions on the element. T_{int} is the integration time, in s. v_0 is the reference velocity, and $v_0 = 1 \times 10^{-9}$ m/s. L_v is expressed in decibels. The velocity level difference $D_{v,ij}$ between element i and j is obtained by

$$D_{v.ij} = L_{v,i} - L_{v,j}\ . \tag{3.5}$$

In the case of transient structure-borne excitation, the normal velocity is needed to be measured instead, and the $D_{v,ij}$ is calculated as follows,

$$D_{v,ij} = \frac{1}{MN}\sum_{m=1}^{M}\sum_{n=1}^{N}\left(D_{v,ij}\right)_{mn} \tag{3.6}$$

where M is the number of excitation positions on element i, N is the number of measurement positions on each element for a single excitation position. $\left(D_{v,ij}\right)_{mn}$ is the velocity difference for one excitation measurement of a pair of measurement positions on element i,j separately, given as

$$\left(D_{v,ij}\right)_{mn} = 10log\left(\frac{\int_0^{T_{int}} {v_{i,mn}}^2(t)dt}{\int_0^{T_{int}} {v_{j,mn}}^2(t)dt}\right) \tag{3.7}$$

where v_i, v_j are the normal velocities measured at positions on the i and j elements. T_{int} is the integration time.

3.1.2.1 Measurement of $D_{v,ij}$

As described in the standard, either a steady-state or transient excitation can be applied to create a vibration field. The basic requirement is the vibration level measured on the receiving component of a joint should be 10 dB higher than the background noise level in each frequency band. In the field measurement of this thesis, the transient excitation by an impact hammer was used.

Hammer hits should be made with about the same strength over a surface area of 1 to 2 m^2 during a time of 20 to 30 seconds. Excitation frequency should be based on 1 to 2 Hz, with high background noise the frequency should be increased. With transient excitation, the average velocity level difference $D_{v,ij}$ should be measured

simultaneously on both the source (on which excitation is applied) and receiving element.

The vibration velocities are to be measured by accelerometers, which are fixed directly on the surface of each element. The ones with adequate sensitivities and low self-noise have to be chosen to ensure a good signal-to-noise ratio, and the mass should be small enough to avoid mass loading which can decrease the measurement accuracy.

On the source plate, a minimum of 4 excitation positions are needed, and on both source and receiving plates minimum of 3 measurement positions each are needed for every excitation. Measurement points should be randomly distributed on the surface of each element. The detail requirement on minimum distances shall be met as 0,5 m between each excitation position and all boundaries of the element in the test; 1,0 m between any two excitation positions; 1,0 m between each excitation position and the junction under test; 1,0 m between each excitation position and the related measurement positions; 0,25 m between each measurement position and the element boundaries; 0,5 m between the different measurement positions for each accompanying excitation position.

3.1.3 Structural reverberation time T_s and its measurement

Structural reverberation time is defined as the time needed for the average velocity or acceleration level in a vibrated structure to drop by 60 dB after the excitation source has stopped. Similar to the reverberation time of rooms, the reverberation time of structures can also be determined by linear extrapolation of a smaller evaluation range than 60 dB.

To measure the structural reverberation time, vibration measurement of point excitation on the structure has to be conducted as referred to in Section 7.3 in ISO 10848-1 [8]). The T_s of the test element is calculated either as the arithmetic average of each individual reverberation time or by energy averaging for all single decay curves.

The method of integrated impulse response will be used to obtain the decay curves following the standard ISO 3382-2 [7]. To be noticed about the decay curve is that only the ones that start not less than 35 dB above the background floor are considered valid. With varied- slope or curved decay, the earlier part is preferred to be evaluated. For low- and mid-frequency ranges, the point of a drop of 3 dB is suggested as the start point with a 5 dB or 10 dB for the evaluation range.

There are also two excitation approaches noted in the standard to obtain the impulse response of test elements - an electrodynamic shaker with an MLS signal or swept sine signal and an impact hammer with a transient signal. The method with impact hammer may have limitations related to the results' accuracy, but due to limited access to instruments and time, the thesis performed the T_s measurement

based on the same procedure for measuring $D_{v,ij}$ from which the time signal of each blow was recorded.

Excitation and measurement positions should follow the requirement as follows: 3 excitation positions at least should be chosen on the test plate, for each excitation position minimum of 3 measurement positions are needed; 0.5 m minimum between each measurement position; 0.5 m minimum between each measurement position with the element boundaries; 1 m minimum between each excitation position and measurement positions.

3.1.4 Measurement limitations

The evaluation of a building component is a complex process, and to be able to get reliable measurement data, guidelines, and detailed requirements are important to follow. There are, however, many unavoidable measurement limitations both practically and theoretically.

3.1.4.1 Practical limitations

In ISO 10848 the requirements on the facility and building element under text are recommended to refer to the ones for the laboratory environment. Practically in the field, the test element is mostly connected with other building structures which in one way can reduce the measured velocity level difference due to involved extra flanking paths, and in another, reflected energy from connected elements can cause variance in measuring the reverberation time and give inaccurate absorption length. During the on-site measurements, time is often a limitation. In this case, to save time, measurements were done in one direction only. Both plates in the joint are made of the same material, so this simplification was judged as not having a significant impact on the results.

3.1.4.2 Theoretical limitations

An applicable and invariant value of K_{ij} is based on the theoretical assumptions made according to the classic SEA (Statistical Energy Analysis) model, which requires that elements under investigation are weakly coupled and the vibration fields of elements are diffuse. While there are uncertain factors or situations that might make the measured K_{ij} irrelevant, which can include: every single element could not be treated as a valid subsystem when strong coupling occurs in the connection; e.g. the structure's high internal damping, the vibration level decreases greatly by distance on the element makes the vibration field not reverberant; low mode count in any one-third octave band as well low modal overlap factor (see section 2.3.3) of the element can affect the measurement accuracy, especially for low frequencies.

3.2 Building structure under investigation

3.2.1 Measurement object, Magasin X

The measurement was performed in Magasin X, a seven-floor office building that was nearly in the finishing stage of construction with all the major work completed. The building locates in Uppsala, at Sidenvävargatan street. Cross-laminated timber is the main material used for the construction, which makes it Sweden's tallest office building in wood and offers 11 000 square meters of office space. Primarily the building was designed to be made with steel and concrete frame [1], but was later changed to wood to reduce the environmental impact and to provide a natural and healthier work environment.

Figure 3.1: The view of Magasin X during the measurement

3.2.2 Materials

On top of the concrete foundation and basement [1], 850 cubic meters of glulam and 3240 cubic meters of cross-laminated timber were used, making wood the main material in the building.

The supplier of cross-laminated timber used in the building is Martinsons [2]. The thickness of plates varies between 180 mm and 270 mm. The most commonly used plates are thicknesses of 200 mm and composed of five layers, for example, the walls on which measurements were performed were 200 mm thick, with 40 mm thick each ply. The minimum strength class for wood slabs used according to the construction drawings of Magazin X is C24, the detailed physical properties of that are described in the theory section, in Table 5.1.

In one of the walls, a hole was cut, which enabled us to empirically confirm the material used. The thickness of the CLT wall was 20 cm, with five laminated layers, which is the same as the material tested in the thesis. The cross-section of CLT used is shown in Figure 3.2.

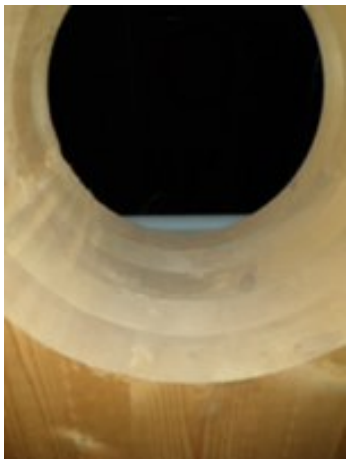

Figure 3.2: One of the CLT walls - showing five visible layers.

3.2.3 The joint structure

The most commonly used types of joints in the building are T-, L-, X-, and inline joints. Two locations on the bottom floor were targeted for taking measurements, they are a wall-wall T-joint in the staircase and a ceiling-wall L-joint by the entrance. The T-joint detail is shown in Figure 3.3a, the left showing the cross-section view, and the right is the vertical section. The demonstration shows the primary joint connection is by the long nails screw. (Though showing in "L-shaped", the joint we measured belongs to the same type but has one wall side extended.) When performing measurements on site, a coupled wall connecting to the T-joint with an external metal plate was also investigated, which we called it in-line joint, the details shown in Figure 3.3b. The L-shaped ceiling joint is made of both fasteners and a beam clued in between the ceiling and wall element, and the ceiling element has thicker layers and higher mass compared to the other two wall joints.

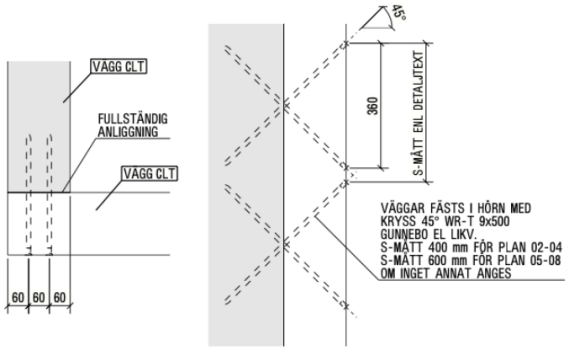

(a) T joint

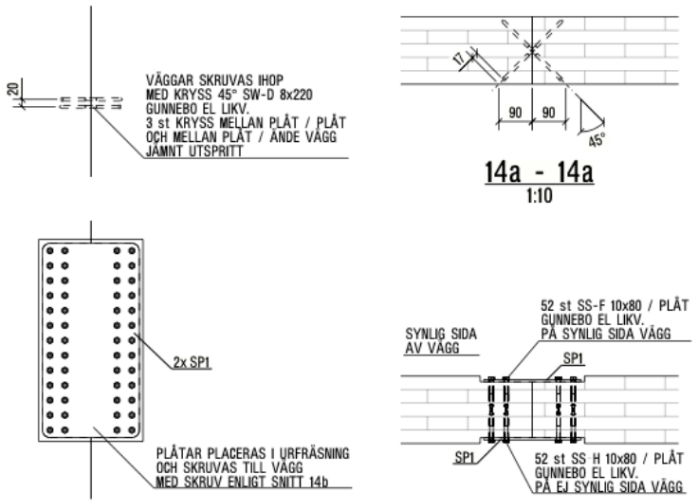

(b) In-line joint

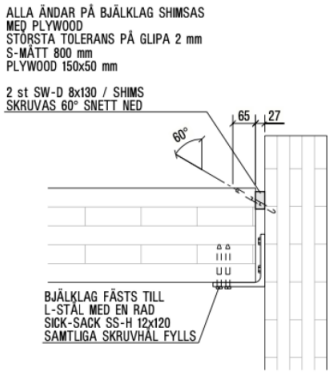

(c) Ceiling joint

Figure 3.3: Construction details of the investigated joints (images are taken from corresponding project documentation.)

3.3 Measurement implementation

3.3.1 Setup on site

All the CLT structure was exposed, enabling easy access and the mounting of accelerometers. Accelerometers with varying sensitivity were used, mounted with beeswax, and secured with duct tape on the wires. Three accelerometers each on both the sending plate and receiving plate were mounted and distributed randomly. The excitation was applied with an impact hammer with a built-in force transducer, a rubber tip was chosen. Four excitation positions were identified randomly on the sending plate. The data acquisition system used for measurements was LMS SCADAS with Simcenter Testlab software on a computer. Accelerometers and an impact hammer were connected to the LMS unit through BNC cables. Specific measurement transducers used are as follows,

1. Force transducer VP 161 (built in the impact hammer), with sensitivity 0.26 mV/N
2. Triaxial accelerometer VP 221, with sensitivity 10.63 mV/ms^{-2}
3. Triaxial accelerometer VP 215, with sensitivity 10.45 mV/ms^{-2}
4. Triaxial accelerometer VP 360, with sensitivity 1.032 mV/ms^{-2}
5. Triaxial accelerometer VP 294, with sensitivity 108 mV/ms^{-2}
6. Triaxial accelerometer VP 487, with sensitivity 105.5 mV/ms^{-2}
7. Triaxial accelerometer VP 461, with sensitivity 102 mV/ms^{-2}.

3.3.2 Implementation

All the measurements on the three joints were performed following the standard ISO 10848-1:2017 [8]. Figure 3.4 shows pictures of joints under investigation, with accelerometers distributed randomly on plates, and cables connected to the LMS unit. The joints' information and basic setup are summarized in Table 3.1 (where Ex.P. and Mea.P. are abbreviations for excitation positions and measurement positions). Other elements such as beams and handrails and lamps are visible, but their influence on the measurement results is hard to evaluate, and thus those elements are neglected in the modeling.

Table 3.1: Measured junctions with the setup.

Joint name	**T joint**	**In-line joint**	**Ceiling Joint**
Elements	Wall→Wall	Wall→Wall	Ceiling→Wall
Length×Width (in m)	0.89×2.9, 1.1×2.9	0.89×2.9, 2.55×2.9	3.1×2.55, 5×2.55
nr. of Ex.P.	4	4	4
nr. of Mea.P.	3 , 3	3 , 3	3 , 3

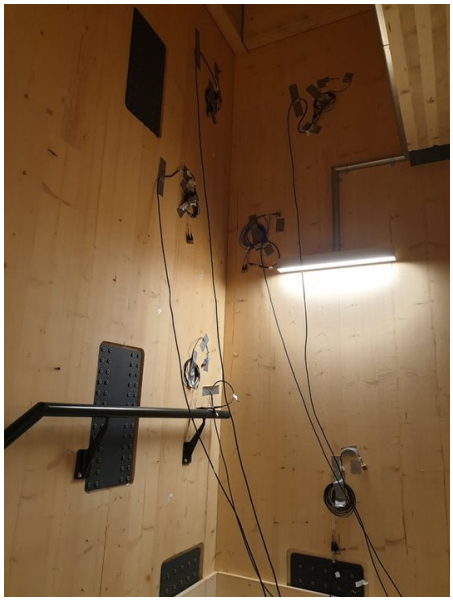

(a) T joint.

(b) In-line joint.

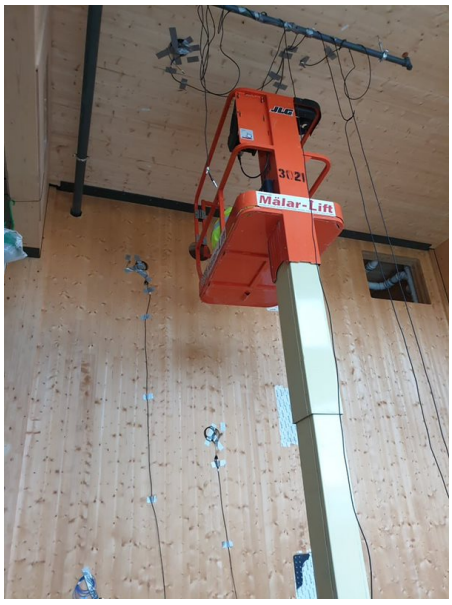

(c) Ceiling joint.

Figure 3.4: Measurement setups for the three joints.

Excitation of the structure was applied with an impact hammer, shown in Figure 3.5. This hammer was relatively lightweight, with a head mass of about 500 g. Rubber tip was used due to the fact that low frequencies were of interest, as well as to prevent CLT from any damage.

Figure 3.5: Impact hammer used for excitation.

Mounting of accelerometers was relatively easy since the CLT was exposed. Beeswax was used for mounting. The cables were secured with duct tape. Accelerometer positions were distributed randomly on the bottom half of the plate. That was the part where access during the measurement was relatively easy, the plate was divided in half with a floor. An exemplary measurement point is shown in Figure 3.6.

Figure 3.6: Example of a measurement point with cables secured by tapes.

4

Measurement results

In this chapter, the measurement results on the three joints i.e. the T joint, the in-line joint, and the ceiling joint will be presented and analyzed. Focused quantities include the measurement coherence, the mobility of the joint structure, the structural reverberation time, and the vibration reduction index.

Coherence is an important indicator to evaluate measurement quality. It reflects how much of the output signal is caused by the input signal as a function of frequency. In general, coherence close to one means that the measurement is reliable. Coherence values might be lower in the range that is close to the eigenfrequencies of influenced modes. The mobility can be used to describe the reaction of a structure on a certain position to the exciting force as well as to determine the anti-resonances of the structure. Usually, the frequencies where the most obvious peaks occur regardless of excitation and measurement positions are the eigenfrequencies of the structure and the dips mostly represent the anti-resonance frequencies which might differ for different excitation and measurement positions. Structural reverberation time is important to calculate the absorption length a_i, a_j and the vibration reduction index $K_{i,j}$ which is used to evaluate the impact of a joint on the energy transfer.

4.1 T joint

4.1.1 Measurement coherence

The measurement coherence on the sending plate of the T-joint is generally good – mostly above 0.8, except for a clear dip occurring at 30∼40 Hz, for all four excitation positions; for the receiving plate, several sharp dips are detected such as around frequencies of 30 Hz, 40 Hz, 90 Hz, and 100 Hz. Most dips can be found correspondingly in the mobility measurement results in Figure **??** which means they are probably related to the mode behavior of the two plates. The generally poor coherence of the measurement on the receiving plate is probably influenced also by the energy transmitted through the junction.

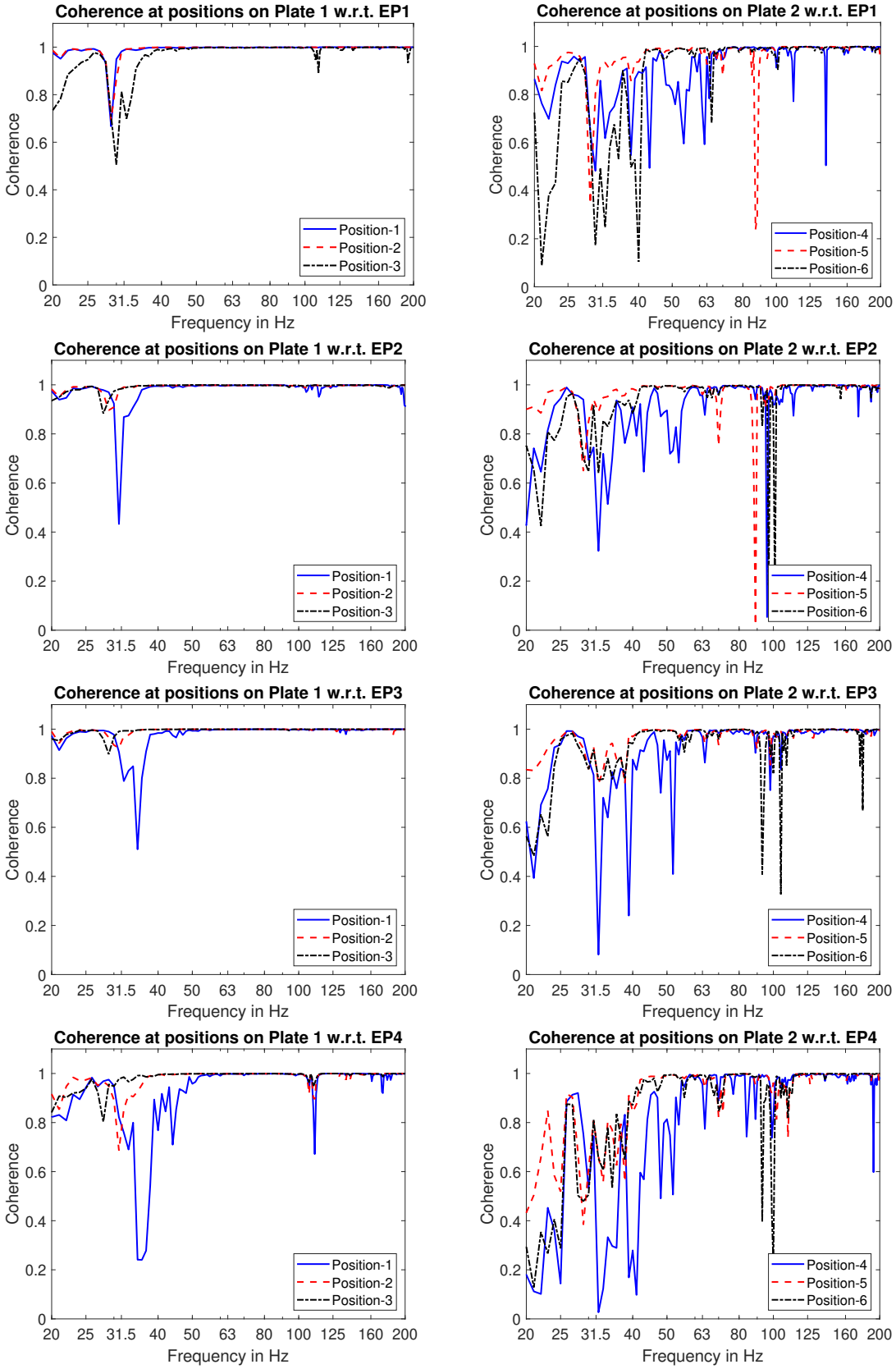

Figure 4.1: Coherence on the measurement of T joint, w.r.t excitation positions EP1-EP4, with sending and receiving plate noted as Plate-1 and Plate-2 respectively.

By comparing the four different excitation position results, the one from excitation position 2 (EP-2) looks better except for the most obvious dips close to 100 Hz. Because of the narrow surface of the plate, EP-1 and -4 are quite close to the boundaries which may cause some uncertainties with respect to the output signal on the receiving plate. Based on the coherence results the valid frequency range would be narrowed down, and certain excitation positions' measurements will be chosen for further analysis.

4.1.2 Mobility measurement

As the mobility results show in Figure 4.3, the mobilities form complicated and rough curves with fluctuations, especially for the receiving plate. For either the sending or receiving plate the different measurement position's results display a general consistent trend of the curve, and about 20 dB mobility level drop from the sending plate to the receiving plate is distinguishable.

The most obvious fact to find is the first peak and dip on the sending plate, with EP-1 and -2, the three measurement positions show great conformity on the resonances around 27 Hz and anti-resonances around 31.5 Hz; with Ep-3 and -4 the anti-resonances for position-3 give a slight shift to higher frequencies at about 35 Hz. For the receiving plate, similar forms of peaks appear at these low frequencies for all the measurement positions which to some extent means that the two plates behave in quite the same way at least at low frequencies. At higher frequencies, the plates behave very differently from this measurement which would take into account their boundary conditions are various, and the transmitted vibration through the junction should also make some other effects.

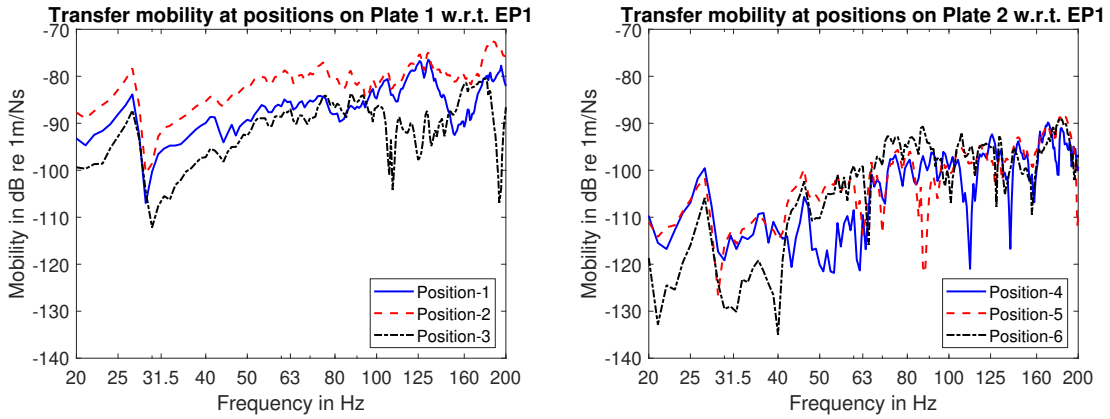

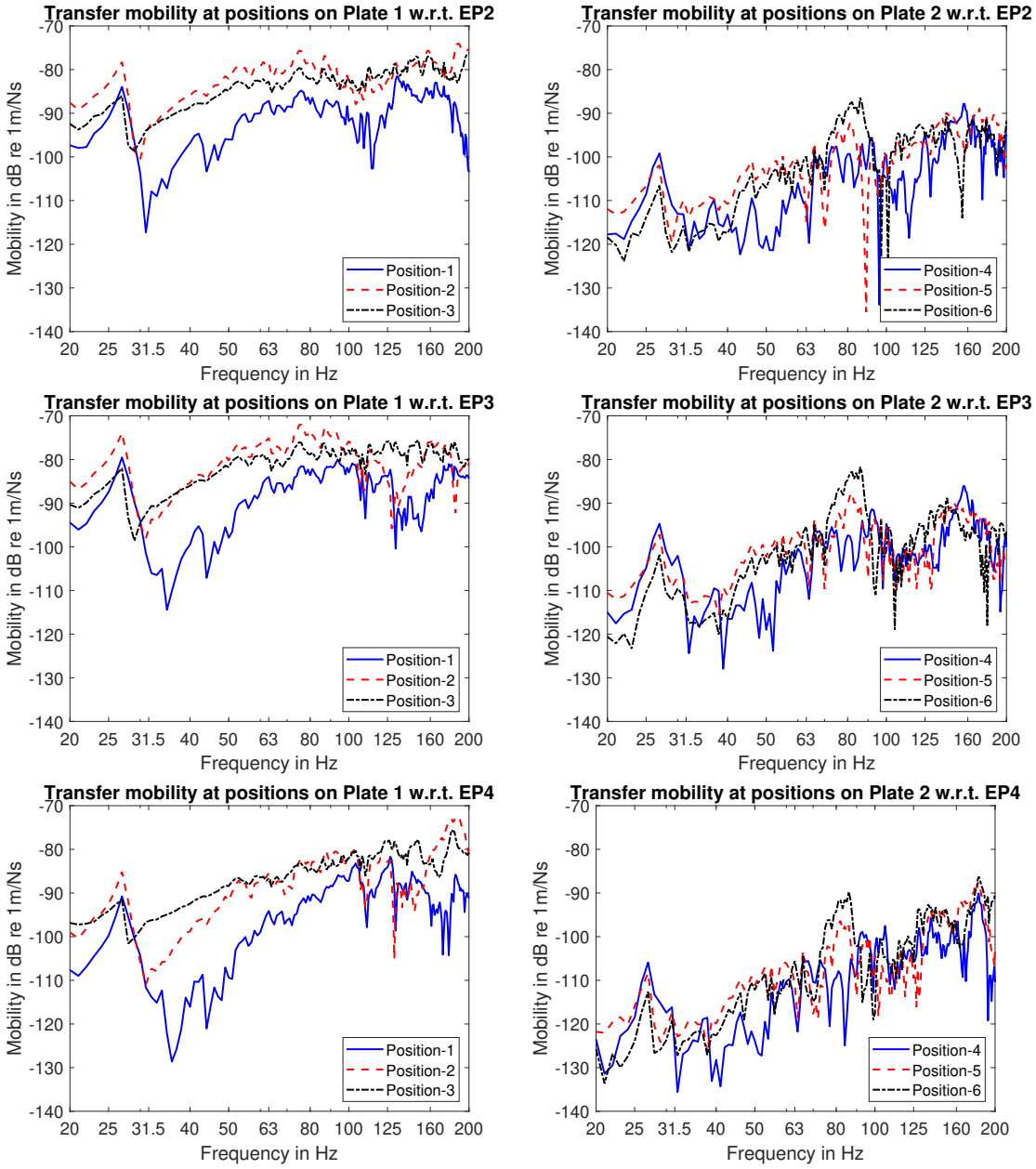

Figure 4.3: Transfer mobilities of T joint, w.r.t excitation positions EP1-EP4, with sending and receiving plate noted as Plate-1 and Plate-2 respectively.

4.1.3 Vibration reduction index

The vibration reduction index calculated for the T-joint in narrow bands and third-octave bands is shown in Figure 4.4. The values of structural reverberation time were assumed to be the same for all the frequencies in the certain third-octave band, which causes sudden changes in values for narrow bands when the band changes. The overall vibration reduction index is quite high, with two dips for 80 Hz and 150 Hz.

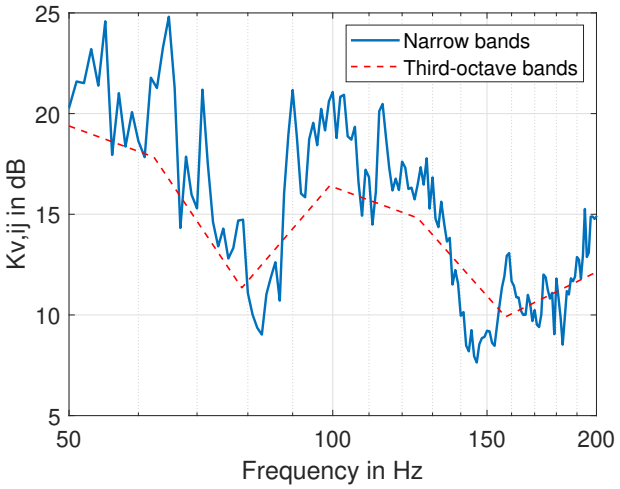

Figure 4.4: Vibration reduction index for the T joint.

4.2 In-line joint

4.2.1 Measurement evaluation

The coherence of the in-line joint measurement is significantly higher than that for the T-joint, especially for the receiving plate. Similarly, as for the T-joint, the lowest coherence occurs for excitation point 4. This point was located close to the bottom edge which could lead to an increased vibration transmission through other paths.

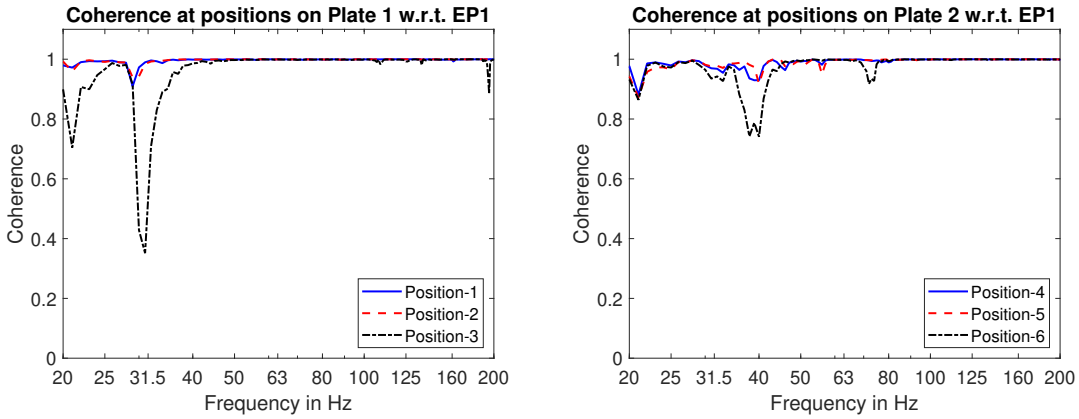

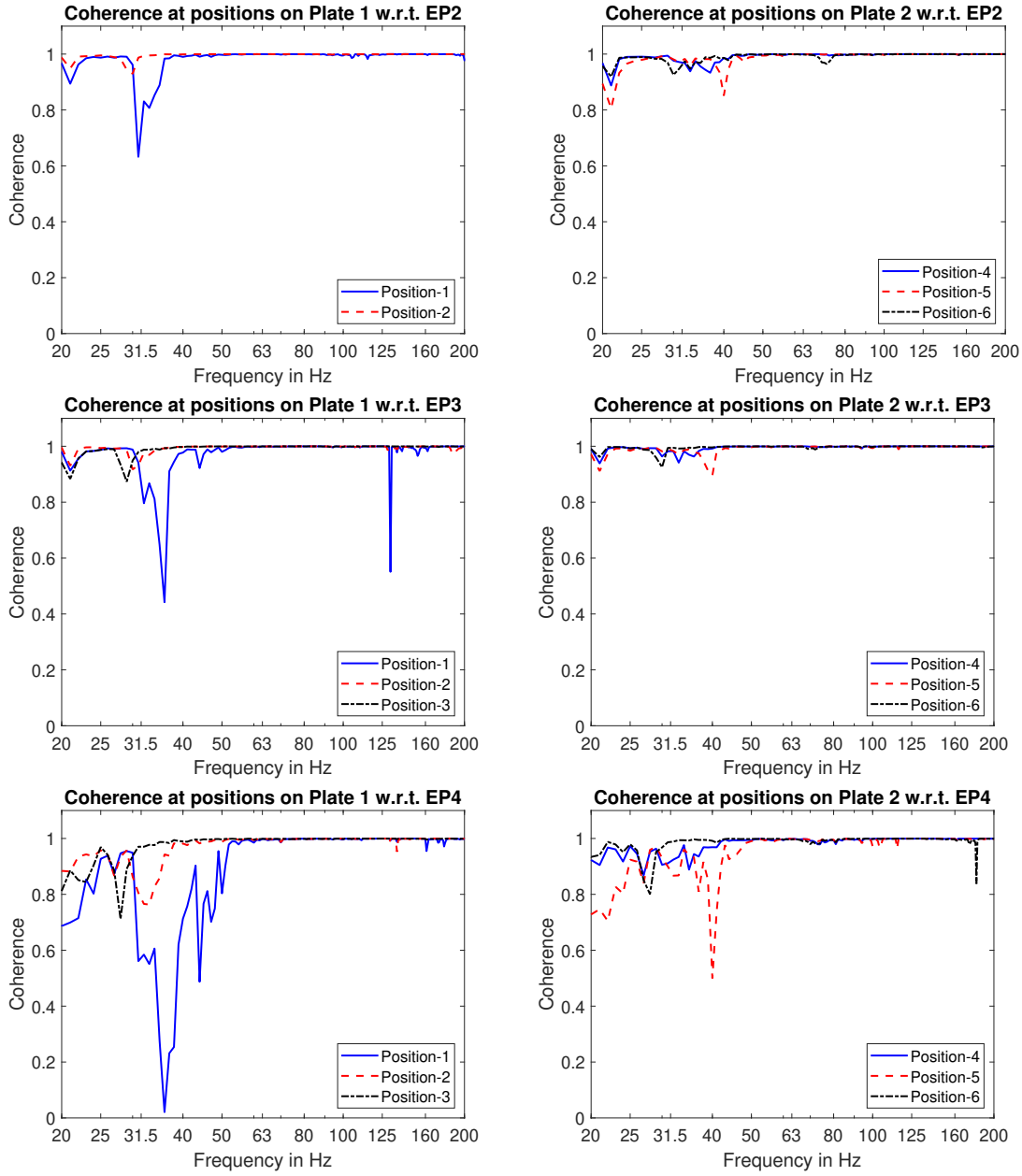

Figure 4.6: Coherence on the measurement of in-line joint, w.r.t excitation positions EP1-EP4, with sending and receiving plate noted as Plate-1 and Plate-2 respectively.

4.2.2 Measured mobilities

Measured mobilities for the receiving plate of the in-line joint are significantly higher than the values measured for the T-joint. In fact, values obtained for the receiving plate are very similar in level to the values for the sending plate. The only reduction in mobility is visible for frequencies around 40 Hz. For the receiving plate, a dip in mobilities occurs, which is not visible for the sending plate. Due to the significant energy transfer, the in-line joint can be treated as a continuous plate.

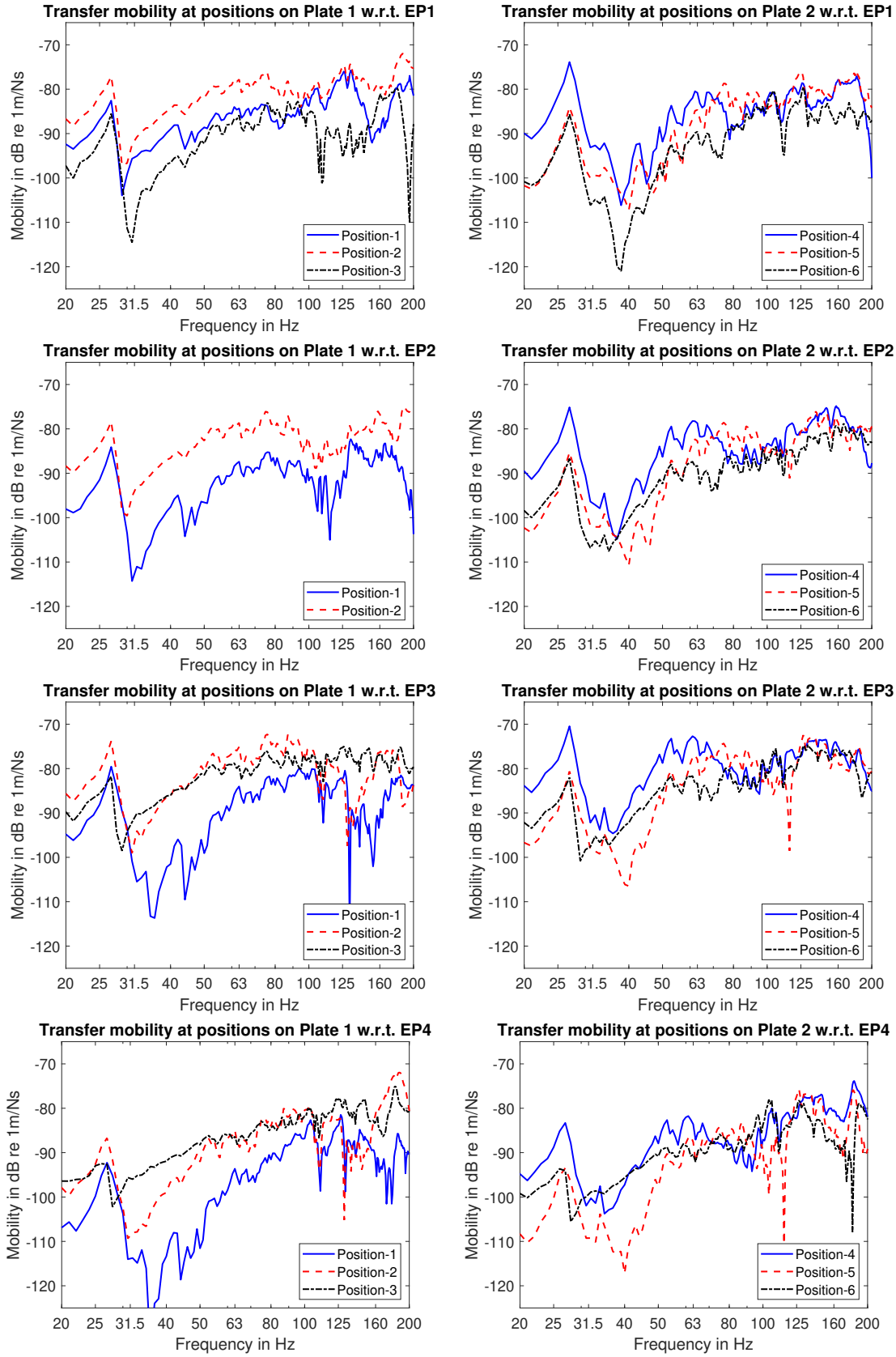

Figure 4.7: Transfer mobilities of in-line joint, w.r.t excitation positions EP1-EP4, with sending and receiving plate noted as Plate-1 and Plate-2 respectively.

4.2.3 Vibration reduction index

The vibration reduction index for the in-line joint is shown in Figure 4.8. The values are negative in the almost whole frequency range, they are positive for frequencies above 100 Hz only. The joint seems to have no impact on vibration propagation, two plates connected with an in-line joint can be treated as one plate. Interestingly, a dip is visible for the frequency at 150 Hz, the same as for T-joint.

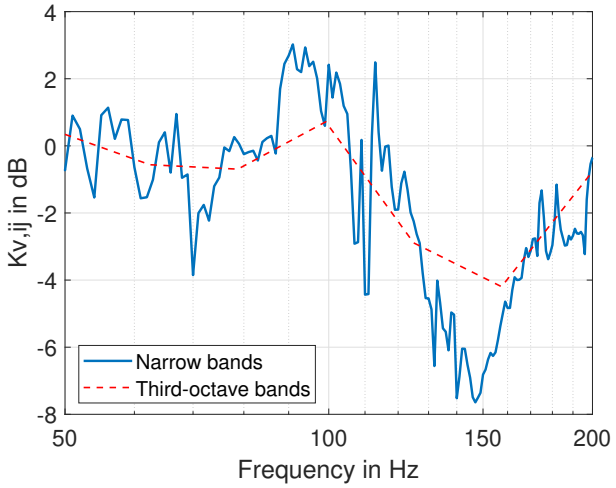

Figure 4.8: Vibration reduction index for the in-line joint.

4.3 Ceiling joint

4.3.1 Measurement evaluation

The coherence for the ceiling joint is quite good for the sending plate, while significantly poor for the receiving plate. Since the low coherence for the receiving plate was observed during the measurement, measurements with extra two excitation positions were tested. The EP-5 and EP-6 were located closer to the joint. The reason for the low coherence might be linked to the complicated joint structure.

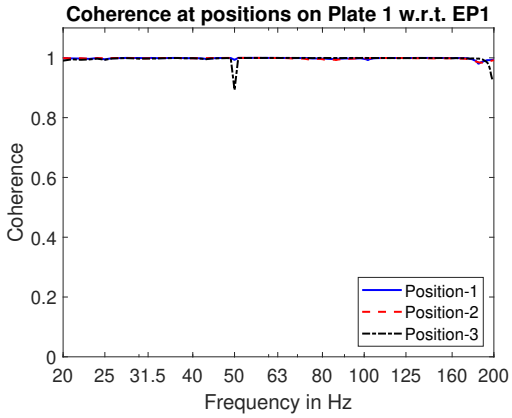
Coherence at positions on Plate 1 w.r.t. EP1
Coherence
Frequency in Hz
Position-1
Position-2
Position-3

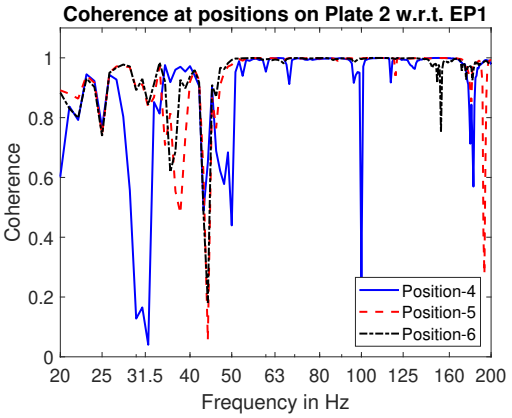
Coherence at positions on Plate 2 w.r.t. EP1
Coherence
Frequency in Hz
Position-4
Position-5
Position-6

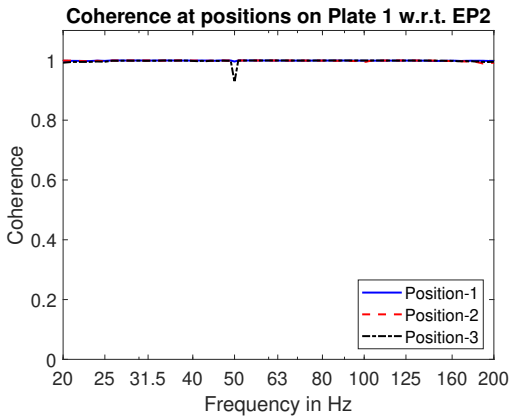
Coherence at positions on Plate 1 w.r.t. EP2
Coherence
Frequency in Hz
Position-1
Position-2
Position-3

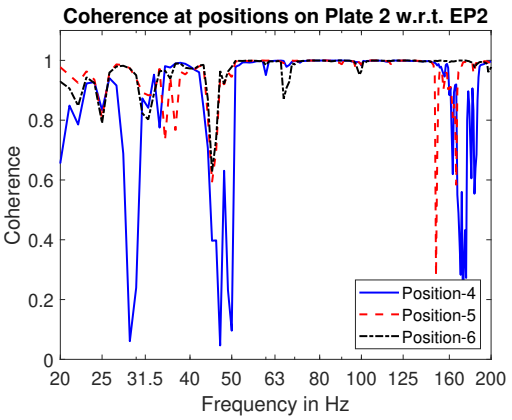
Coherence at positions on Plate 2 w.r.t. EP2
Coherence
Frequency in Hz
Position-4
Position-5
Position-6

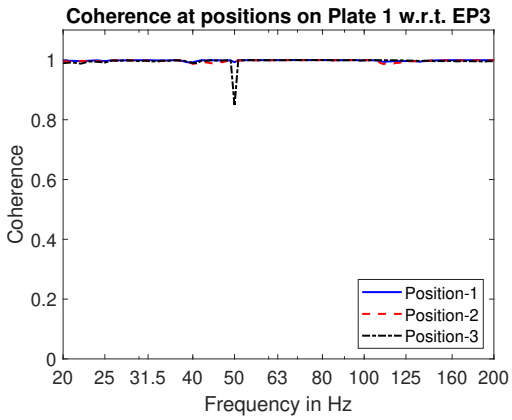
Coherence at positions on Plate 1 w.r.t. EP3
Coherence
Frequency in Hz
Position-1
Position-2
Position-3

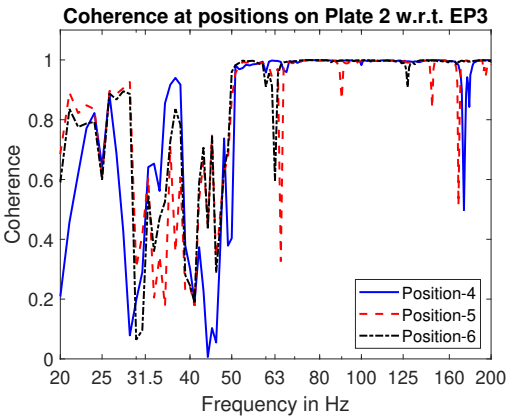
Coherence at positions on Plate 2 w.r.t. EP3
Coherence
Frequency in Hz
Position-4
Position-5
Position-6

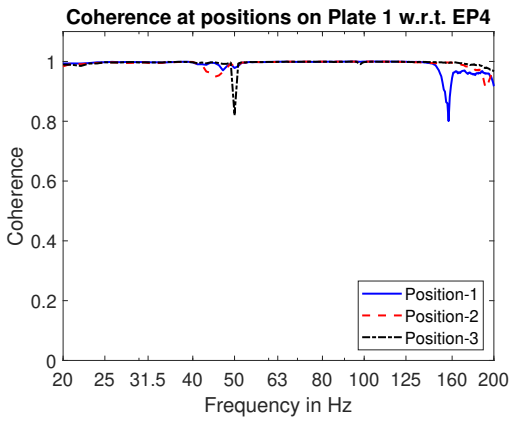
Coherence at positions on Plate 1 w.r.t. EP4
Coherence
Frequency in Hz
Position-1
Position-2
Position-3

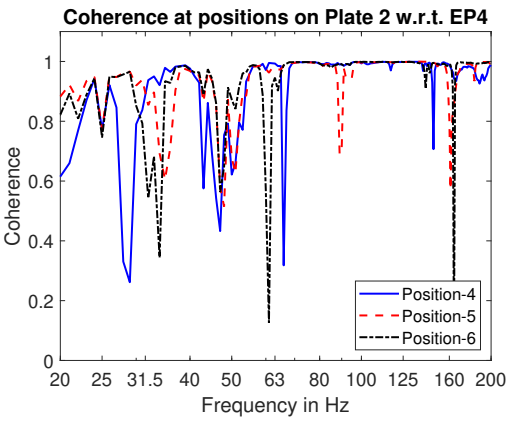
Coherence at positions on Plate 2 w.r.t. EP4
Coherence
Frequency in Hz
Position-4
Position-5
Position-6

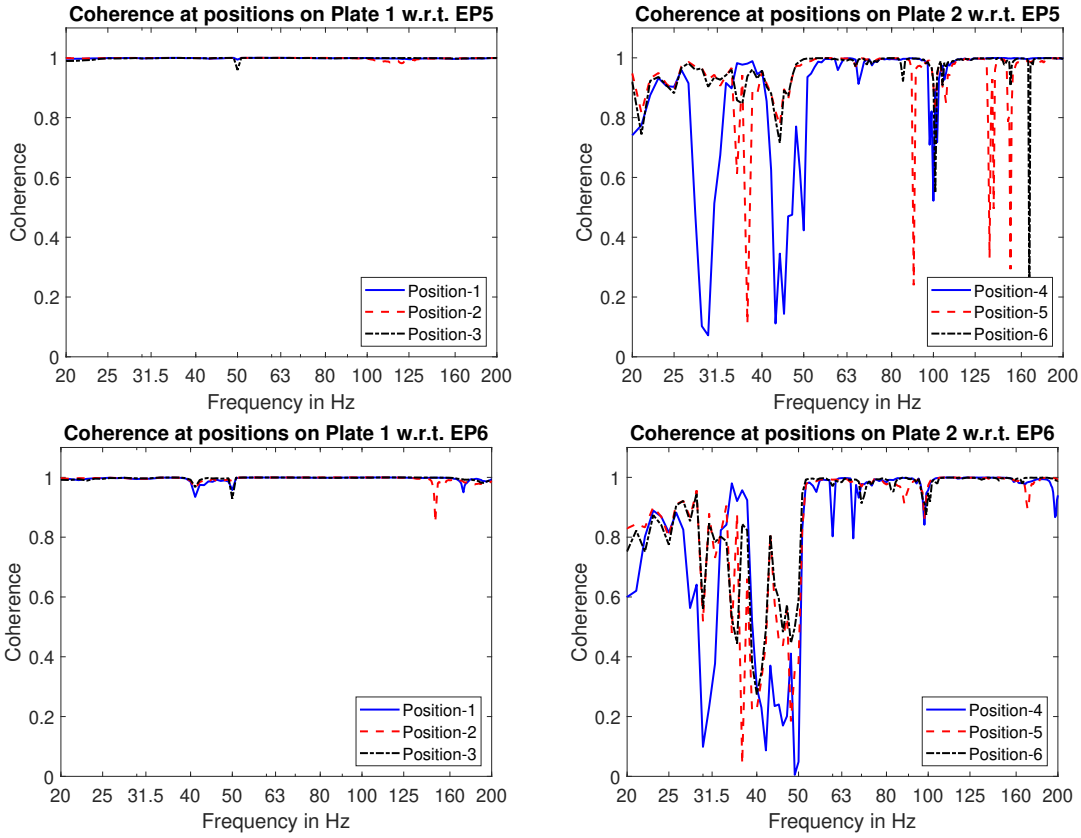

Figure 4.10: Coherence on the measurement of ceiling joint, w.r.t excitation positions EP1-EP6, with sending and receiving plate noted as Plate-1 and Plate-2 respectively.

4.3.2 Measured mobilities

For the ceiling joint measured mobilities for the sending plates have fewer sharp peaks and dips than for the T-joint and in-line joint, the curves are more smooth. The ceiling plate might be more damped than the wall plates. The thickness of the CLT used for the floor is 270 mm, while CLT used for walls is 200 mm thick, which might lead to higher damping for the ceiling. Another reason might be the fact that the construction of the ceiling is simpler, and there is less impact on other structures, such as beams. The frequency dependence of mobilities for the receiving plate, which is a wall, is similar to for the in-line and T-joint, with significant, narrow peaks and dips.

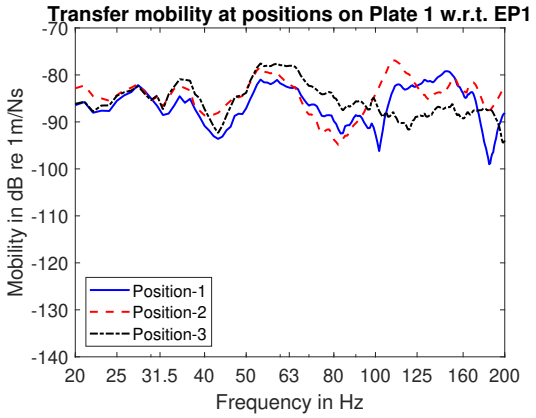
Transfer mobility at positions on Plate 1 w.r.t. EP1
Mobility in dB re 1m/Ns
Frequency in Hz
Position-1
Position-2
Position-3

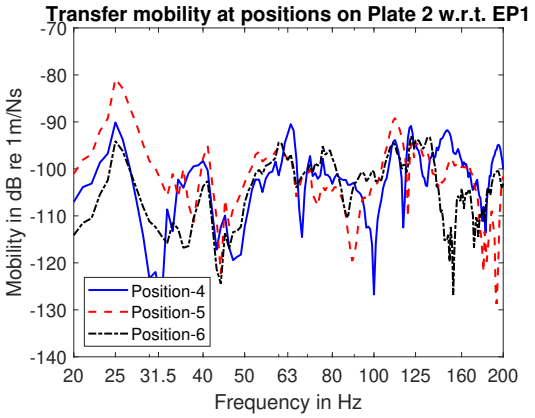
Transfer mobility at positions on Plate 2 w.r.t. EP1
Mobility in dB re 1m/Ns
Frequency in Hz
Position-4
Position-5
Position-6

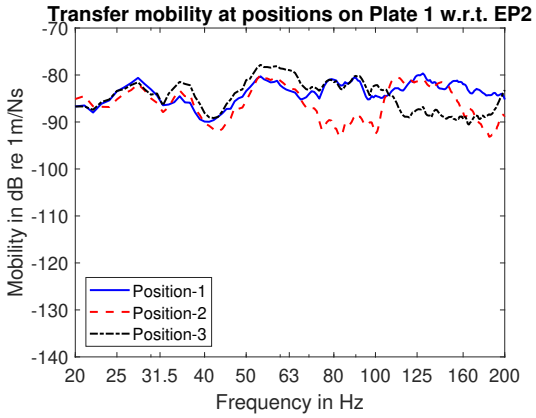
Transfer mobility at positions on Plate 1 w.r.t. EP2
Mobility in dB re 1m/Ns
Frequency in Hz
Position-1
Position-2
Position-3

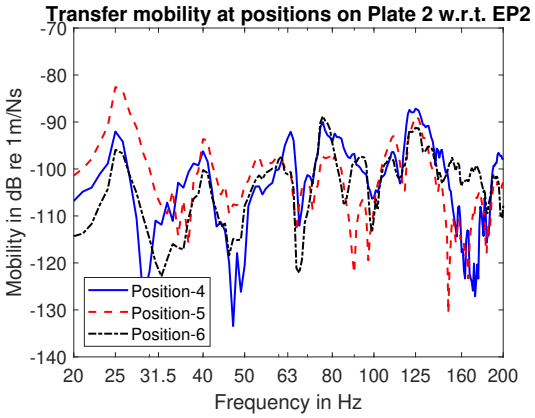
Transfer mobility at positions on Plate 2 w.r.t. EP2
Mobility in dB re 1m/Ns
Frequency in Hz
Position-4
Position-5
Position-6

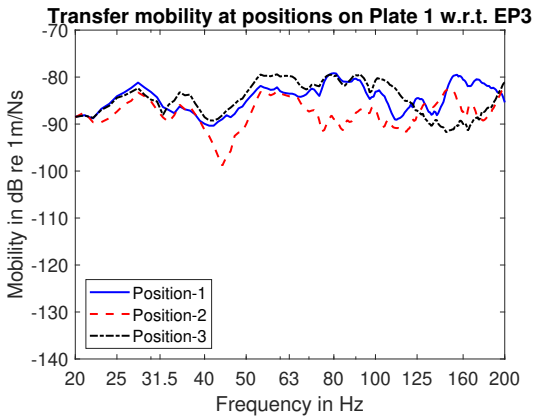
Transfer mobility at positions on Plate 1 w.r.t. EP3
Mobility in dB re 1m/Ns
Frequency in Hz
Position-1
Position-2
Position-3

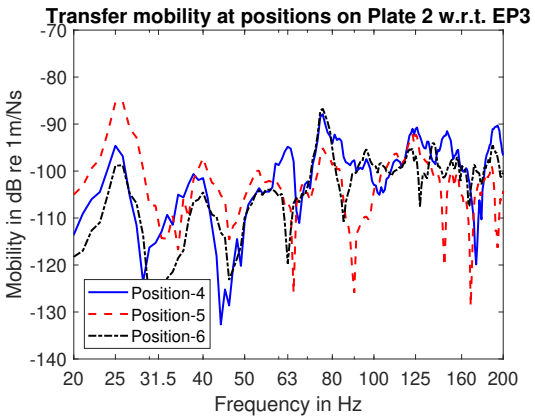
Transfer mobility at positions on Plate 2 w.r.t. EP3
Mobility in dB re 1m/Ns
Frequency in Hz
Position-4
Position-5
Position-6

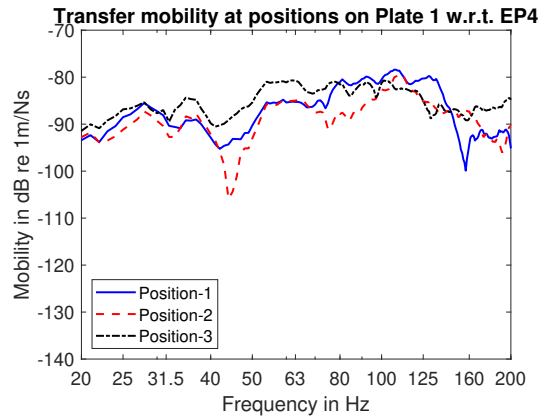
Transfer mobility at positions on Plate 1 w.r.t. EP4
Mobility in dB re 1m/Ns
Frequency in Hz
Position-1
Position-2
Position-3

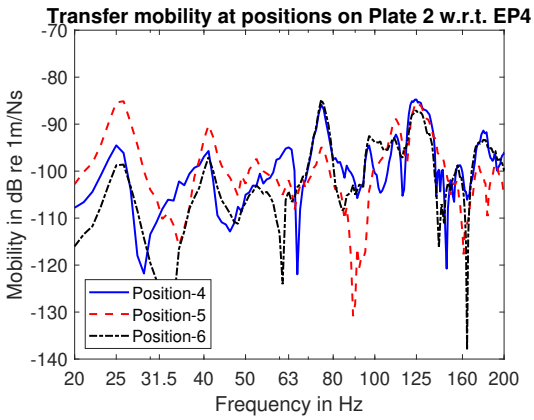
Transfer mobility at positions on Plate 2 w.r.t. EP4
Mobility in dB re 1m/Ns
Frequency in Hz
Position-4
Position-5
Position-6

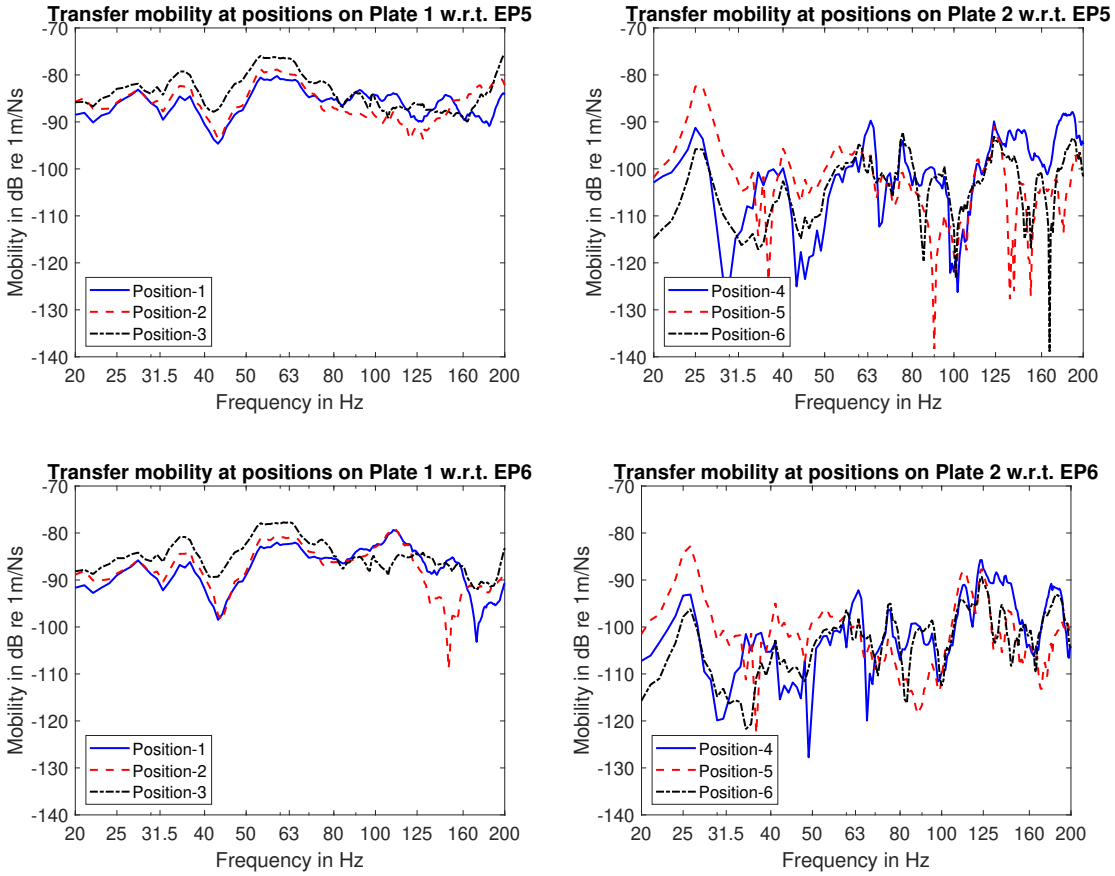

Figure 4.12: Transfer mobilities of ceiling joint, measured from the four sets of excitation positions EP1-EP4, Plate-1 and -2 represent sending and receiving plate respectively.

4.3.3 Vibration reduction index

The vibration reduction index for the ceiling joint is shown in Figure 4.13. The construction of the joint is more complicated than the previous two, which makes it difficult to identify the impact of individual components. A dip is visible for frequency 80 Hz, similarly as for the T-joint.

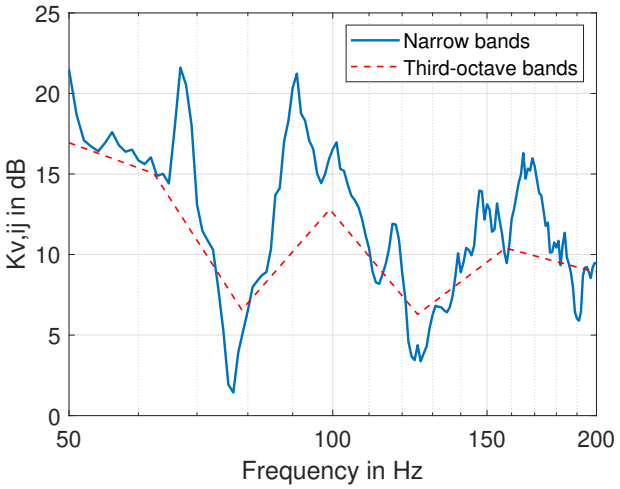

Figure 4.13: Vibration reduction index for the ceiling joint.

4.4 Structural reverberation time

During the measurement, a relatively lightweight impact hammer was used, which reduced the amount of energy used for excitation. Due to this, the decay visible in decay curves was low. To evaluate reverberation time, the decay by 10 dB was used.

f [Hz]	RT [s]
50	0.67
63	0.60
80	0.34
100	0.52
125	0.47
160	0.25
200	0.21
250	0.10

Table 4.1: Measured structural reverberation time.

4.5 Vibration reduction index

High vibration reduction index values mean that little energy is transferred. In Figure 4.14 vibration transmission index for a T-joint, in-line joint, and ceiling joint were compared. Results are plotted for third-octave bands. For the in-line joint obtained vibration reduction index is significantly lower than for two other types of joints, which means that vibrations can propagate easily. The in-line joint can be approximated as a continuous plate because of the high energy transfer.

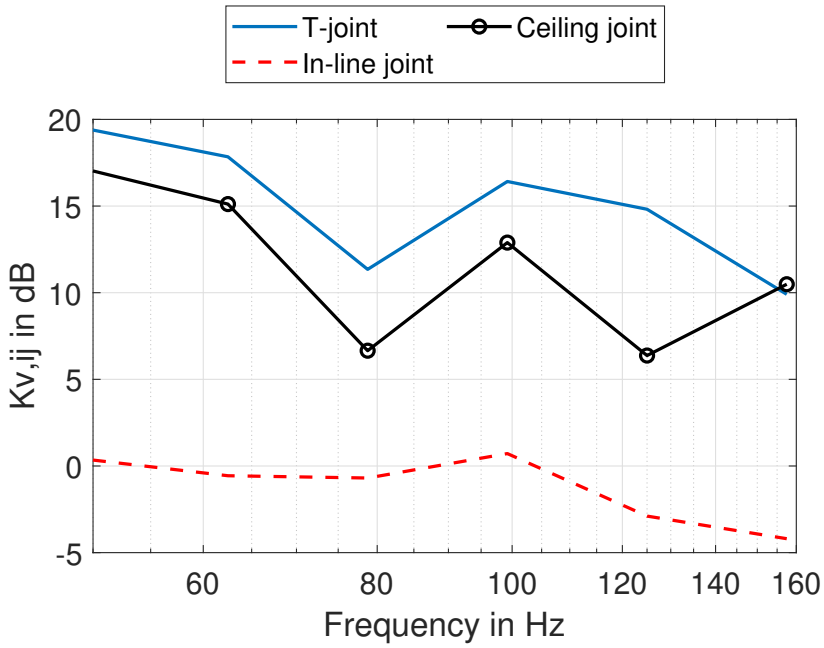

Figure 4.14: Comparison of vibration reduction index values for different joints

The highest vibration reduction index is achieved for the T-joint, in the whole frequency range. Construction of the T-joint was much simpler than the ceiling joint, it contains two plates screwed together. Ceiling joint construction included a metal bracket and plywood distancing part, as shown in Figure 3.3c. In such constructions, elastic interlayers are commonly used to reduce the vibration propagation [12]. The load is also different for the ceiling joint, where just the vertical plate is under load, while for the T joints, both plates experience the same load.

For both the T-joint and ceiling joint, the highest vibration transmission loss occurs for the lowest frequencies. Since the reverberation time is the highest for low frequencies, which leads to the lowest loss factor, low-frequency vibrations are expected to be propagated the easiest. Low frequencies are also identified as problematic for lightweight constructions. This result might be caused by low power input to the structure, because of the use of a lightweight modal hammer.

5

Finite element model

5.1 Background

The Finite Element Method is one of the numerical methods used to determine a structure's behavior in certain conditions. In principle, a complicated structure is divided into a number of small elements, which are way easier to analyze. A continuous structure is approximated as a discrete one [15]. Differential equations are formulated for each element. Then equations for elements are coupled, with the equilibrium and continuum conditions applied in connection points and boundary conditions applied for boundaries. The system of equations is solved, giving solutions in connection points and boundaries, from which values for elements can be estimated.

The selection of finite elements can affect the simulation results. To achieve great accuracy, it is usually recommended to define elements so that there are at least three to six elements per wavelength [3]. A common technique is varying the element size, to save computational power. Smaller elements are defined in areas with more complex behavior, such as close to boundaries, while bigger elements are sufficient for other parts of the structure.

In the project, the application COMSOL was used to study the CLT element. The simulations described in this chapter were done in COMSOL Multiphysics 5.6, Solid Mechanics module was applied.

5.2 Modeling of exemplary plate

FEM modeling was initially done with a simple CLT plate including trials of e.g. the basic parameter settings and mesh settings to simulate the modes and the frequency responses. A reference thesis work [18] was studied and compared in this section, and two modeling approaches including solid plate and shell were tested. Since the purpose is to evaluate the simulation technique, the size of the plate was set the same as in the reference thesis, hence it is different than in the final model.

The exemplary structure was given the dimensions of 6 m by length, and 3 m by width. It has a total thickness of 20 cm, composed of 5 CLT layers with each single ply thickness of 4 cm. The orthotropic material properties and stiffness properties were all set the same as in the referred thesis (which actually has coincidently the

same parameter settings as the final joint model as in Table 5.1).

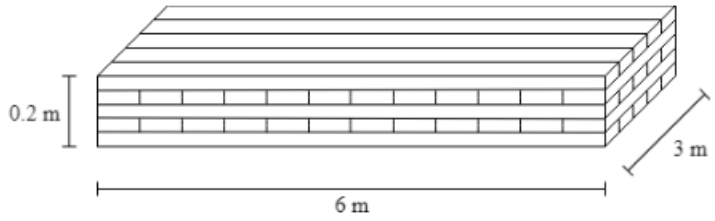

Figure 5.1: Sketch of the modeled CLT panel [18].

5.2.1 Solid plate approach

Solid mechanics module is applied in this approach. Layers of ply are built from 1 to 5 directly on each other as presented in Figure 5.2. Layers 1st, 3rd, and 5th have the major timber grain direction on the x-axis and the minor direction on the y-axis. Layers 2nd and 4th were built oppositely for the timber grain direction. The model is simulated with simply supported boundary conditions on the two short edges of the panel i.e. along the y-axis, and defined on the middle plane in the thickness direction. These basic model information and boundary constraints were set the same as the reference thesis.

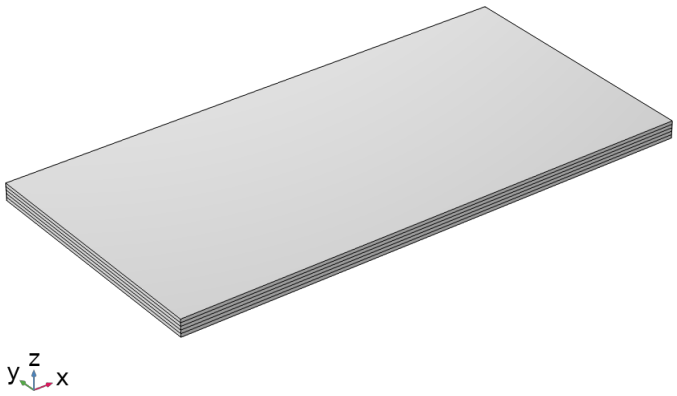

Figure 5.2: The solid CLT plate model with five internal layers.

The different scales of element size in mesh mapping and element division in the thickness direction were tested to make more comparisons. As a result, the element size in extremely fine predefinition, and the distribution of two elements per layer in the thickness direction was chosen, which got closer simulation results in both the modes frequencies and the corresponding shapes as regards the same modeling approach result in the reference work. Figure 5.5 displays the obtained first eight eigenfrequencies.

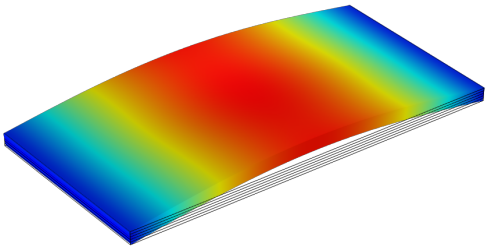

(a) 1st eigenfrequency at 10.97 Hz.

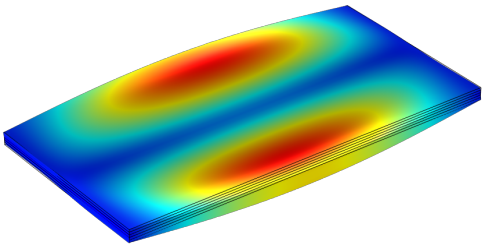

(b) 2nd eigenfrequency at 14.81 Hz.

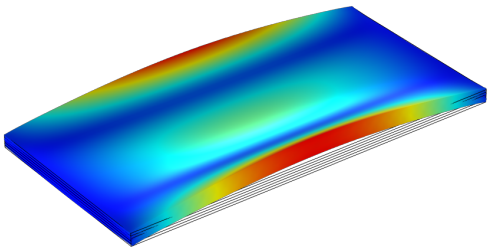

(c) 3rd eigenfrequency at 24.45 Hz.

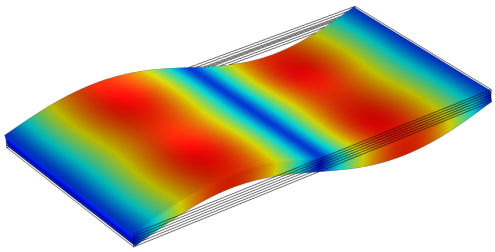

(d) 4th eigenfrequency at 38.82 Hz.

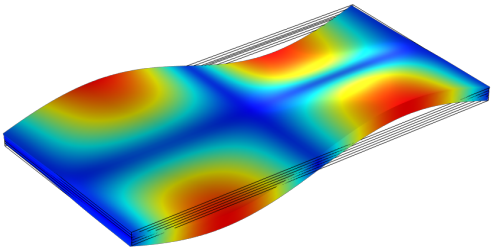

(e) 5th eigenfrequency at 43.54 Hz.

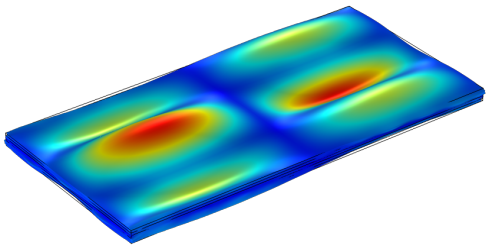

(f) 6th eigenfrequency at 48.69 Hz.

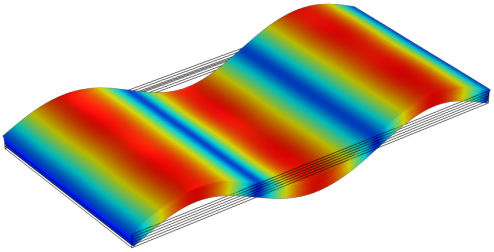

(g) 7th eigenfrequency at 75.1 Hz.

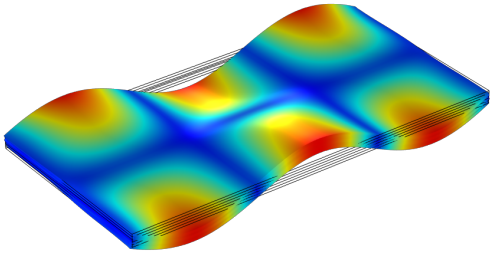

(h) 8th eigenfrequency at 79.53 Hz.

Figure 5.3: Mode shapes of the solid CLT model – first eight eigenfrequencies.

5.2.2 Shell approach

Again the same CLT element with the same dimensions and material composition was modeled in the shell approach. Though the *shell* model looks like having no thickness information, there is actually 3D composition of layers with all the orthotropic properties included. The frequency's location and shape of modes got much closer results than the solid approach study. For example, it got exactly the same mode shapes for all eigenfrequencies while the solid model got deviations for the 3rt until the 5th mode. Though the shell approach enables significantly reduces the computation time and obtained more validated mode study results, we decided to proceed with the solid approach because the shell model has higher challenges and more unknowns in modeling the joint details.

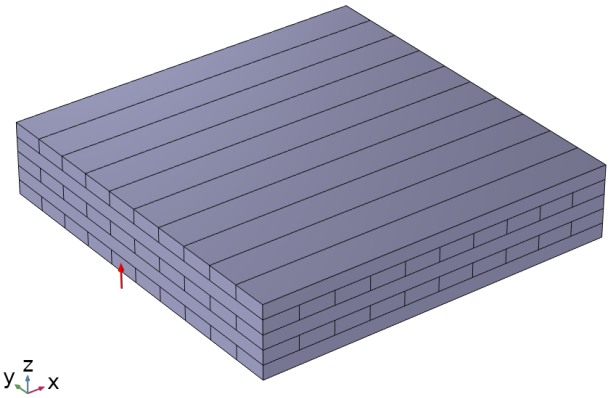

(a) 3D layer stack in the shell model.

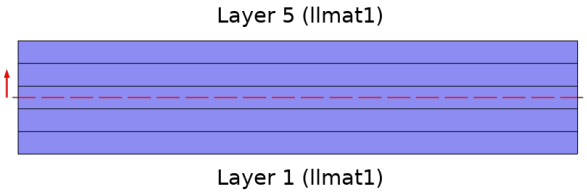

(b) Profile of the layer stack.

Figure 5.4: The shell CLT model showing in shell properties.

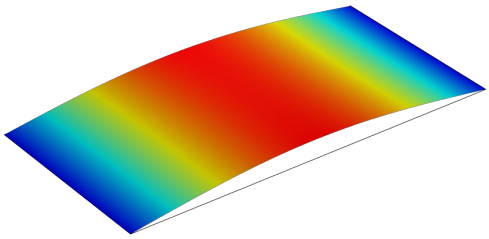

(a) 1st eigenfrequency at 11.02 Hz.

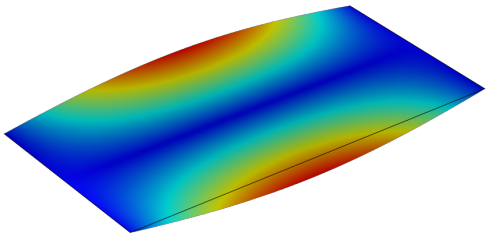

(b) 2nd eigenfrequency at 16.13 Hz.

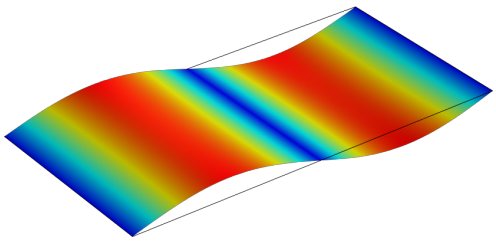

(c) 3rd eigenfrequency at 38.97 Hz.

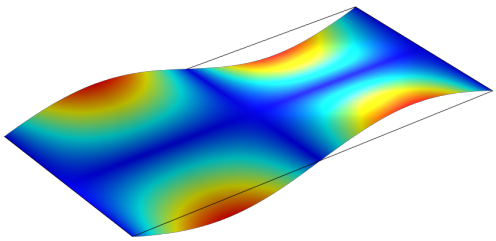

(d) 4th eigenfrequency at 44.16 Hz.

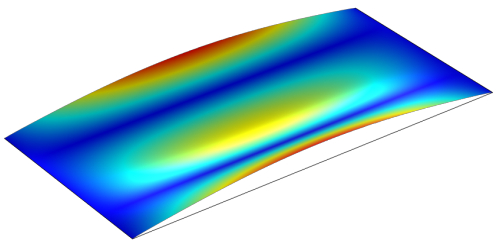

(e) 5th eigenfrequency at 56.26 Hz.

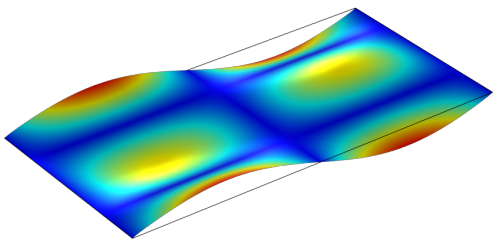

(f) 6th eigenfrequency at 73.99 Hz.

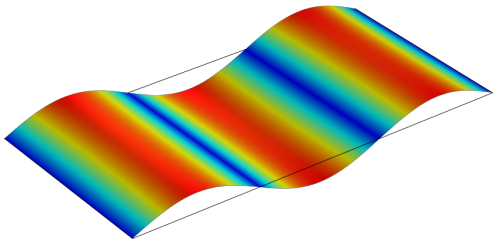

(g) 7th eigenfrequency at 75.11 Hz.

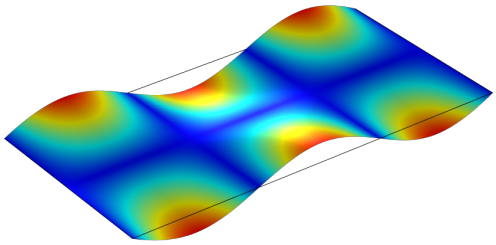

(h) 8th eigenfrequency at 79.81 Hz.

Figure 5.5: Mode shapes of the shell CLT model – first eight eigenfrequencies.

5.3 The T-joint model

5.3.1 Parameter settings

The model was built directly in COMSOL environment. Because of its simplicity, this method was chosen to provide easy access to each element, which could be more complicated with the geometry imported from other software.

A T-joint of two CLT plates was modeled to simulate the wall-corner joint. Each plate consists of five-ply layers, modeled separately. Each layer was 40 mm thick. Figure 5.6 shows projections of the modeled joint, done in AutoCAD. Dimensions of elements are given in millimeters.

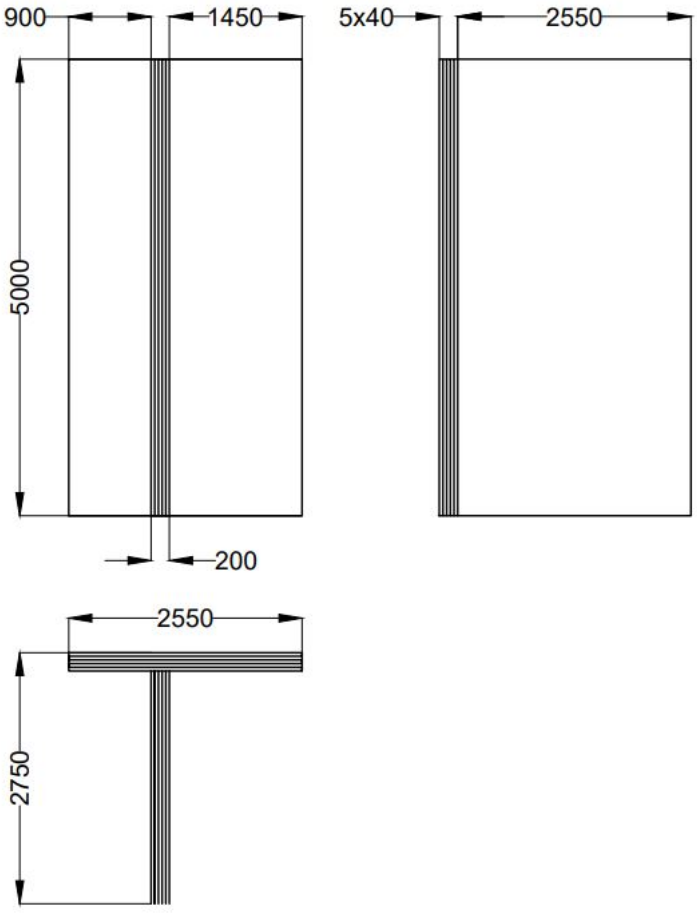

Figure 5.6: Projections of the T joint

A view of the model done in COMSOL is shown in Figure 5.7 below. The points marked on the model are excitation and measurement points, defined to simulate the measurement described in the next chapter.

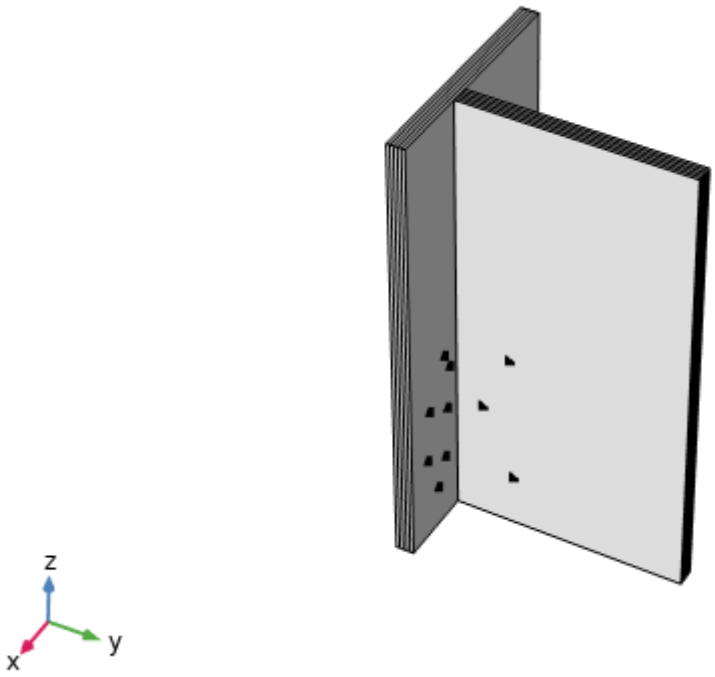

Figure 5.7: T joint model in COMSOL

The material of the model is a linear elastic material, with orthotropic properties applied. The material properties are set following the CLT strength class used in the measured structure i.e. C24. The Young's moduli, shear moduli, and Poisson's ratios in three orthogonal axes as well as material density are shown in Table 5.1. And the loss factor for orthotropic Young's modulus η_E and for shear modulus η_G was also defined as the total loss factor calculated based on structural reverberation time (according to the Equation 2.35), with the assumption that all three directions x, y and z have identical value.

Table 5.1: Material parameters of CLT joint model in COMSOL.

E_L	1.1^{10} Pa
E_R	3.7^{8} Pa
E_T	3.7^{8} Pa
G_{LR}	6.9^{8} Pa
G_{RT}	5.0^{7} Pa
G_{LT}	6.9^{8} Pa
μ_{LR}	0.51
μ_{RT}	0.31
μ_{LT}	0.38
ρ	420 kg/m^3
η_E	0.08
η_G	0.08

To simulate the measurement, point load was applied on defined points. The type

of load was a total force of 1 N, applied in the direction perpendicular to the board.

Boundary conditions were applied as *Rigid connector* in COMSOL, enabling prescribing of rotation and displacement in each direction separately. A more detailed study of applied boundary conditions is shown in the next section.

Since the joint is on the ground floor of a seven-story building, the load was applied to show real-life conditions. The load was approximated based on the building's technical documentation. Self-weight of the building in the joint is 100 kN/m, according to the documentation. In the model, the applied load was 120 kN/m, with 20% of the self-weight added for other elements in the building.

5.3.2 Boundary conditions study

Boundary conditions are an important factor in the accuracy of FEM results. Defining boundary conditions that show real-life behavior can be challenging in more complex applications. The basic boundary conditions are either free or fixed for the displacement and rotation, in the dimensions that the structure contains.

During the study, different boundary conditions were examined to obtain the most accurate results. Due to the complicated properties of a real-life building, some simplifications were necessary for the model. Simulations were conducted for three different boundary condition cases, named briefly:

- Simply supported
- Fully restrained
- Combination of pinned and rolled constraints

Mobility obtained for one representative position in the receiving plate (with respect to one excitation position) was compared with the measured mobility (for the same excitation and receiving position). The model with boundary conditions enabling the best fit was selected for further simulations.

The boundary conditions are described in detail in the table below. For each surface boundary conditions were described either as free, or as constrained ("0" in the table) for displacement in x-, y-, and z-direction, as well as for rotation in respective directions.

Table 5.2: Simply supported boundary conditions

Surface	Disp x	Disp y	Disp z	Rot x	Rot y	Rot z
A	free	free	free	free	free	free
B	free	free	free	free	free	free
C	free	free	free	free	free	free
D	free	free	free	free	free	free
E	free	free	free	free	free	free
F	0	0	0	0	0	0
G	0	0	0	0	0	0

Table 5.3: Fully restrained boundary conditions

Surface	Disp x	Disp y	Disp z	Rot x	Rot y	Rot z
A	0	0	0	0	0	0
B	0	0	0	0	0	0
C	0	0	0	0	0	0
D	0	0	0	0	0	0
E	0	0	0	0	0	0
F	0	0	0	0	0	0
G	0	0	0	0	0	0

Table 5.4: Combination of pinned and rolled constraints

Surface	Disp x	Disp y	Disp z	Rot x	Rot y	Rot z
A	free	free	0	free	free	free
B	0	0	0	free	free	free
C	free	free	0	free	free	free
D	0	0	0	free	free	free
E	free	free	0	free	free	free
F	0	0	0	free	free	free
G	0	0	0	free	free	free

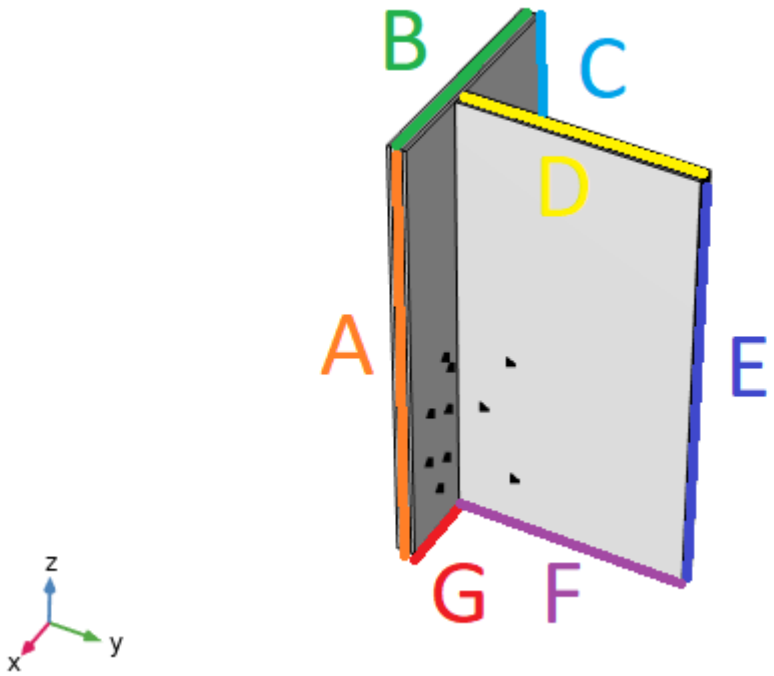

Figure 5.8: Symbols used for boundary conditions description

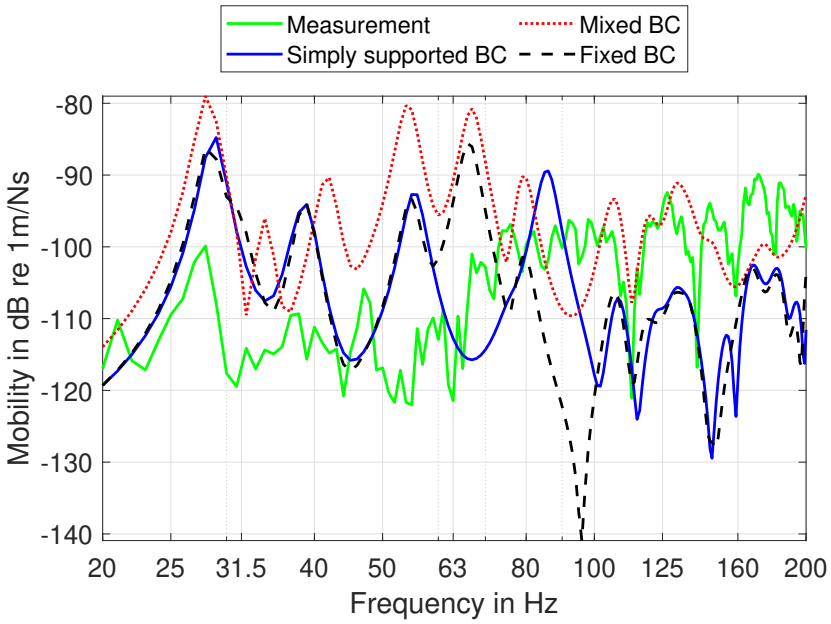

Figure 5.9: Boundary condition study

The accuracy of boundary conditions was evaluated by comparing the mobility on the receiving plate with measurement results. The 27 Hz peak, which is the first eigenfrequency of a single plate, is clearly visible for all three boundary conditions. For fixed boundary conditions, a significant dip in mobility occurs for 95 Hz, which is not the case for the measurement results. Modal density is also significantly lower for the simply supported and fixed boundary conditions. For mixed boundary conditions, modal density is slightly higher, and the fit for frequencies above 80 Hz is fairly good. Mixed boundary conditions were chosen for further simulations, even though the mobilities for frequencies 80 Hz were higher than for the measurement results.

5.3.3 The modes of single joint element

A separate model the single plate of the joint was also built to determine which modes are visible in the measurement. Since the two elements of the joint are identical (even in dimensions), studying the modes' behavior of a single plate is also accessible and necessary. The boundary condition is set the same as the combination of pinned and rolled constraints in the above subsection i.e. all the boundary surfaces are free in terms of rotation along all the orthogonal, the top and bottom surfaces are fully restrained in terms of displacement while the two side surfaces' displacement only constrained along the z-axis. The load setting is neglected for this modeling. Figure 5.10 shows the first few mode shapes and their frequencies.

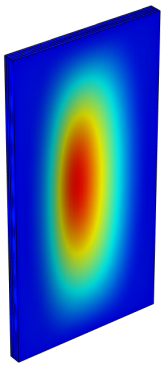

(a) 1st eigenfrequency at 27 Hz.

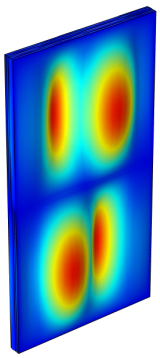

(b) 2nd eigenfrequency at 51.32 Hz.

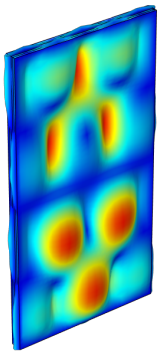

(c) 3rd eigenfrequency at 68.6 Hz.

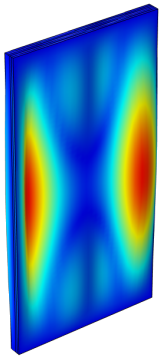

(d) 4th eigenfrequency at 112.78 Hz.

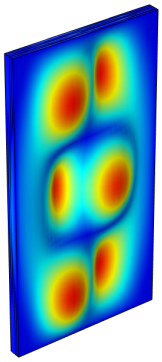

(e) 5th eigenfrequency at 122.6 Hz.

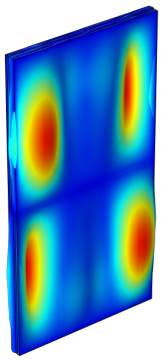

(f) 6th eigenfrequency at 139.18 Hz.

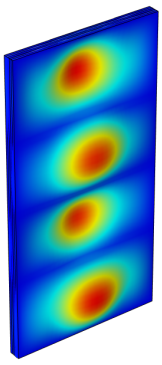

(g) 7th eigenfrequency at 163.67 Hz.

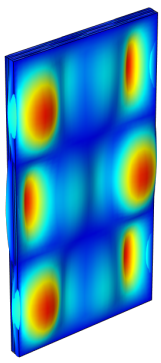

(h) 8th eigenfrequency at 179.2 Hz.

Figure 5.10: Mode shapes of one element in the joint – first eight eigenfrequencies

The first eigenfrequency of 27 Hz can be clearly seen in both the measured mobility evaluation of the T-joint in Section 4.1.2 and simulation results above in Figure 5.9. As one of the most significant mobility peaks, it demonstrates that this first eigenfrequency dominates the joint's behavior critically. There are also some other peaks that match the frequencies of the modes, for example, around 126 Hz, and above 160 Hz, for both measurement and simulation results. And when only examining the measured mobilities, a few distinguishable dips at 112 Hz, 139 Hz, and 179 Hz can also be depicted in the single plates modes, probably because the excitation position of that particular run lay on the nodes of these frequencies modes.

The T joint modal density is high, which makes distinguishing individual modes above 27 Hz difficult. The second eigenfrequency of 51 Hz can also be seen for the in-line joint. Eigenfrequencies of a single plate seem to dominate the structure's behavior for low frequencies, with the increase of frequency the complexity of the structure becomes visible, and the modal density increases.

5.3.4 Analysis of vibration reduction index

For the calculation of the vibration reduction index, $K_{v,ij}$ velocities obtained from the FEM model was used, but structural reverberation time values were taken from the measurement. The velocities for different excitation positions were averaged by applying all four excitations at the same time in the model.

The vibration reduction index for frequencies below 100 Hz is close to or below 0 dB. This is a consequence of imperfect modeling, with higher than measured mobilities. The connection between plates is modeled as perfect, which is probably too simplified. In reality, less energy is transferred from the sending to the receiving plate.

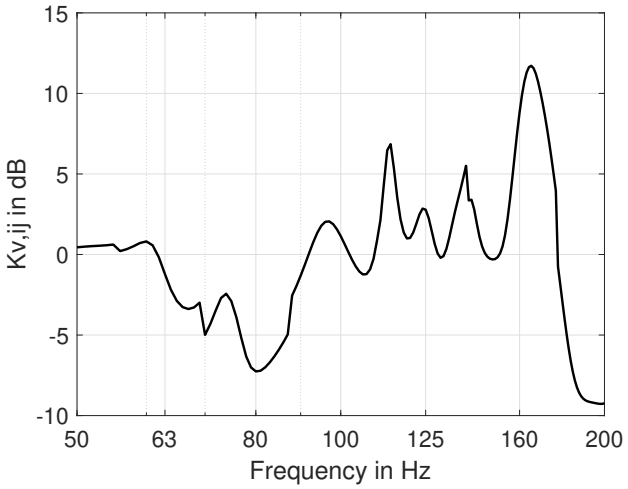

Figure 5.11: Vibration reduction index for the FEM model

6

Discussion

6.1 FEM model

The finite element model of the structure turned out to be difficult to establish correctly. The biggest challenges were correct boundary conditions and applying orthotropic properties to the structure. The impact of boundary conditions is significant, which is shown in Figure 5.9. The fact that the measurements were done in the building makes the selection of the correct BC more difficult, as real-life BC was complicated.

To increase the accuracy of the CLT plate model, each layer was modeled separately, as an orthotropic material. Since the next layers are rotated by 90 degrees, material properties had to be rotated, too. It was found that correct modeling in COMSOL might be problematic, as the order of material properties interferes with the direction of individual layer definitions. Incorrectly defined material properties lead to unevenness in the structure, abnormal looking, and small bumps. A relatively easy way to model orthotropic properties in COMSOL correctly is to define an individual base vector system for each element's orientation, which was done in the thesis.

The model was evaluated by a comparison of mobilities obtained by the measurement and simulation. An exemplary point on the receiving plate was chosen for comparison. Results are shown in Figure 5.9. The model does not describe the structure's behavior perfectly, but the overall agreement regarding levels is acceptable, especially for higher frequencies, above 80 Hz. Despite that, the vibration reduction index varies for simulation and measurement, as shown in Figure 6.1. The vibration reduction index calculated for simulation results shows agreement with theory, contrary to measurement results. As explained above, the vibration reduction index is expected to increase with frequency.

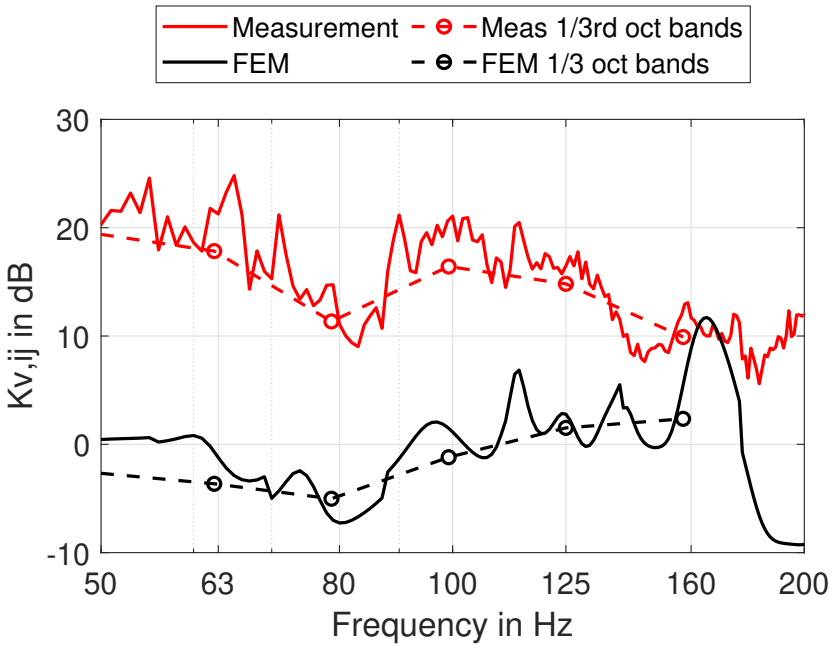

Figure 6.1: Vibration reduction index comparison - Measurement results vs. FEM simulation results

6.2 Structural reverberation time and loss factor

Measured structural reverberation time is shown in Table 4.1. Reverberation time was calculated based on the time signal registered by accelerometers. Each recording consists of ten excitations, leading to ten decay curves, from which the strongest excitation was chosen. Reverberation time was calculated for each receiving point on the sending plate and for each excitation position, and the results were averaged. The total loss factor was calculated for each individual reverberation time and then averaged. Since the loss factor in COMSOL is a single value, the obtained result was averaged in the frequency domain too. The total loss factor is 0.08, which is a value that is also mentioned in literature [4].

7
Conclusion and future works

Detailed investigation and knowledge of a practical construction are highly needed to be able to set the simulation model as accurately as possible. For example, to correctly define the joint element and presume the boundary and load conditions, would require some help from the constructors, this is what we missed on one of the most interesting parts of the thesis. The practical and experience limitations on measuring real structure from us as students have also affected the accuracy.

Cross-laminated timber, as a material built with orthotropic plates, turned out to be difficult to accurately simulate in COMSOL. When the model is set properly regarding material properties and boundary condition estimation, it gives reliable results, even for a significantly simplified joint, for frequencies above 80 Hz. Correct selection of boundary conditions affects the quality of the results.

The mobility measurements of the T joint and in-line joint have demonstrated that the sending and receiving elements have very similar dynamic performance - similar curve shapes and trends, and the single plate's simulation results show the modes influence a lot on the joint's behavior. This further in a way confirmed the measurement results and simulation fit each other, especially in terms of the material properties and modeling method.

The bad coherence on the receiving plate of the T joint and ceiling joint gives a conclusion that the vibration has been greatly influenced when it's passing through the junction, especially below 50 Hz, and so it is worth studying the topic of flanking transmission over a joint in an even lower frequency range. Due to higher mobilities for the receiving plate in simulation results than in measurement results, a different approach to modeling the joint might be of interest for frequencies below 50 Hz.

T joint has a higher measured vibration reduction index meaning it has lower vibration transmission than the ceiling joint in frequencies up to 200 Hz, which would be because the totally rigid connection of the T joint works better than the semi-rigid and indirect connection of the ceiling joint. It is also interesting that though the three types of the joint have different junction details, the measured vibration reduction index $K_{i,j}$ follows a quite consistent tendency in the investigated range.

Relevant future work on the topic could include testing the structure with different weights and tip materials of hammers. Especially for large CLT structures heavier hammers can be required to be able to apply excitation effectively. Besides, the

study (and simulation) of boundary conditions as well as connection details are also definitely important and imperative.

Bibliography

[1] Magasin x materials description. https://www.byggvarlden.se/darfor-bytte-magasin-x-fran-betong-till-tra/. Accessed: 2022-01-12.

[2] Magasin x project description. https://www.tyrens.se/sv/projekt/byggnader/magasin-x-sveriges-stoersta-kontorshus-i-trae/. Accessed: 2022-01-12.

[3] Carl Hopkins. *Sound Insulation*. Elsevier Ltd, 2007.

[4] Antonino Di Bella and Milica Mitrovic. Acoustic characteristics of cross-laminated timber systems, 7 2020.

[5] Carl Hopkins. Sound insulation in buildings: linking theory and practice. In *Proceedings of the Acoustics 2012 Nantes Conference*, 2012.

[6] Jesper Hörnmark. Acoustic performance of junctions in cross laminated timber constructions, 2019.

[7] International Organization for Standardization. ISO 3382-2:2008, Acoustics - Measurement of room acoustic parameters - Part 2: Reverberation time in ordinary rooms, 2008.

[8] International Organization for Standardization. ISO 10848-1:2017, Acoustics - Laboratory and field measurement of flanking transmission for airborne, impact and building service equipment sound between adjoining rooms - Part 1: Frame document, 2017.

[9] International Organization for Standardization. ISO 12354-1:2017, Building acoustics - Estimation of acoustic performance of buildings from the performance of elements - Part 1: Airborne sound insulation between rooms, 2017.

[10] Wolfgang Kropp. Propagation and radiation of structure borne sound, 2015.

[11] L. Cremer, M. Heckl, Björn A. T Petersson. *Structure-Borne Sound*. Springer-Verlag Berlin and Heidelberg GmbH Co. K, 2005.

[12] Martinsons. Materialguide för KL-trä, 2021.

[13] Mendel Kleiner. *Acoustics and Audio Technology*. J Ross Publishing, 2011.

[14] F. Morandi, S. De Cesaris, M. Garai, and L. Barbaresi. Measurement of flanking transmission for the characterisation and classification of cross laminated timber junctions. *Applied Acoustics*, 141:213–222, 12 2018.

[15] O. C Zienkiewicz, R. L. Taylor, J. Z. Zhu. *The Finite Element Method: Its Basicks and Fundamentals*. Butterworth-Heinemann, 2013.

[16] Svenskt Trä. The CLT Handbook CLT structures-facts and planning, 5 2019.

[17] T.E. Vigran. *Building Acoustics*. Taylor & Francis Group, 2008.

[18] Johannes Wetterholt. Modelling cross-laminated timber floors in dynamic analysis - Eigenfrequency prediction, 2019.

DEPARTMENT OF SOME SUBJECT OR TECHNOLOGY
CHALMERS UNIVERSITY OF TECHNOLOGY
Gothenburg, Sweden
www.chalmers.se

CHALMERS
UNIVERSITY OF TECHNOLOGY